G. J. Boer · G. Flato · D. Ramsden

A transient climate change simulation with greenhouse gas and aerosol forcing: projected climate to the twenty-first century

Abstract The potential climatic consequences of increasing atmospheric greenhouse gas (GHG) concentration and sulfate aerosol loading are investigated for the years 1900 to 2100 based on five simulations with the CCCma coupled climate model. The five simulations comprise a control experiment without change in GHG or aerosol amount, three independent simulations with increasing GHG and aerosol forcing, and a simulation with increasing GHG forcing only. Climate warming accelerates from the present with global mean temperatures simulated to increase by 1.7 °C to the year 2050 and by a further 2.7 °C by the year 2100. The warming is non-uniform as to hemisphere, season, and underlying surface. Changes in interannual variability of temperature show considerable structure and seasonal dependence. The effect of the comparatively localized negative radiative forcing associated with the aerosol is to retard and reduce the warming by about 0.9 °C at 2050 and 1.2 °C at 2100. Its primary effect on temperature is to counteract the global pattern of GHG-induced warming and only secondarily to affect local temperatures suggesting that the first order transient climate response of the system is determined by feedback processes and only secondarily by the local pattern of radiative forcing. The warming is accompanied by a more active hydrological cycle with increases in precipitation and evaporation rates that are delayed by comparison with temperature increases. There is an "El Nino-like" shift in precipitation and an overall increase in the interannual variability of precipitation. The effect of the aerosol forcing is again primarily to delay and counteract the GHG-induced increase. Decreases in soil moisture are common but regionally dependent and interannual variability changes show considerable structure. Snow cover and sea-ice retreat. A PNA-like anomaly in mean sea-level pressure with an enhanced Aleutian low in northern winter is associated with the tropical shift in precipitation regime. The interannual variability of mean sea-level pressure generally decreases with largest decreases in the tropical Indian ocean region. Changes to the ocean thermal structure are associated with a spin-down of the Atlantic thermohaline circulation together with a decrease in its variability. The effect of aerosol forcing, although modest, differs from that for most other quantities in that it does not act primarily to counteract the GHG forcing effect. The barotropic stream function in the ocean exhibits modest change in the north Pacific but accelerating changes in much of the Southern Ocean and particularly in the north Atlantic where the gyre spins down in conjunction with the decrease in the thermohaline circulation. The results differ in non-trivial ways from earlier equilibrium $2 \times CO_2$ results with the CCCma model as a consequence of the coupling to a fully three-dimensional ocean model and the evolving nature of the forcing.

1 Introduction

The future or projected climate change simulations discussed here extend to the end of the twenty-first century, that is, to the year 2100. The forcing scenario used is a modified version of the IPCC IS92a scenario following Mitchell et al. (1995). The projected GHG forcing increase is represented by an increase in equivalent CO_2 concentration of 1% per year and an associated change in the distribution and magnitude of sulfate aerosol loading. A description of the coupled model used, and its control climate, is given in Flato et al. (2000). The experimental design of the climate change simulations and the comparison of results with the instrumental record of temperature and precipitation from 1900 to 1995 is discussed in Boer et al. (2000) hereinafter BFRR. The GHG forcing increase, compared to the decade of the 1980s, is equivalent to a doubling of CO_2 near the year

G. J. Boer (✉) · G. Flato · D. Ramsden
Canadian Centre for Climate Modelling and Analysis,
Atmospheric Environment Service,
University of Victoria, BC, Canada
E-mail: George.Boer@ec.gc.ca

2050 and a tripling of CO_2 near the year 2100 in this scenario. Note however, that these times correspond to a tripling and a quadrupling of CO_2 compared to preindustrial control run values. These times are given special attention in the analysis. Equilibrium $2 \times CO_2$ simulations with the same atmospheric model coupled to a simple mixed layer ocean are discussed in Boer et al. (1992) and the effects of aerosol forcing in this equilibrium context in Reader and Boer (1997).

The recent past has been a period with of increasing GHG forcing which is partially compensated by the increase in the offsetting aerosol forcing as discussed in BFRR. The overall rate of climate change is simulated to accelerate during the twenty-first century. A number of two-century simulations with a forcing scenario similar to that used here are available. In addition to the simulation discussed in Johns et al. (1997), and Mitchell and Johns (1997), some information from a simulation at MPI is given in Cubash et al. (1996), and a report of a simulation to 2065 with the GFDL model is given by Haywood et al. (1997).

2 Data and data availability

A rather complete history of both the atmosphere and ocean is retained from the five simulations undertaken. Several special surface data sets together with selected free atmosphere quantities are available for applications and other investigations via the internet at *http:www.cccma.bc.ec.gc.ca* and also through the IPPC Data Distribution Centre. The variables chosen here as the primary climatic variables for the investigation of simulated future climate change include surface air temperature, precipitation, evaporation, mean sea level pressure, soil moisture, and snow and sea-ice. For the ocean, temperature and stream function changes are discussed.

Surface air temperature is a measure of the surface energy budget and is a robust climate parameter in the sense that it is comparatively large-scale, has modest variability, and responds to changes in forcing with a signal which is comparatively large compared to its natural variability. Precipitation and evaporation are measures of the hydrological cycle but precipitation is much less robust than temperature in the sense used here. Precipitation exhibits comparatively small scales, is highly variable, and its forced climate signal is relatively weak compared to its natural variability. It is a primary meteorological variable of considerable practical importance.

Soil moisture is a poorly observed climatic parameter and its representation in climate models is not without ambiguity. Nevertheless, it provides an indication of possible changes in surface hydrology which could have important practical consequences. Changes in the amount and distribution of snow and sea-ice are also of potential practical importance, reflect the evolution of the cryosphere with changes in climate forcing, and are important to the albedo feedback mechanism. They are robust indicators of climate change in most models.

Mean sea-level pressure is a measure of both thermodynamical and dynamical balances at the surface. It is more robust than precipitation but less so than temperature in the sense used already. Changes in mean sea-level pressure are an indication both of large scale changes to the flow including both the direction and strength of the near surface geostrophic wind.

Ocean variables, excepting surface temperature, are comparatively poorly known and are often given less attention in climate warming simulations. The oceanic temperature change with depth, the change in thermohaline overturning, and changes in barotropic flow are discussed here.

A climate change simulation (or observations of the system) produces a time evolving three-dimensional distribution of temperature and other climate variables. The result for temperature, as an example, may be written as $T = T_0 + T_f + T''$ where T_0 is the deterministic climate mean temperature for the system in equilibrium with its (preindustrial) forcing, T_f is the deterministic climate change caused by changes in forcing, and T'' is internally generated natural climate variability. The control simulation is intended to represent the equilibrium climate state $T = T_0 + T'$ while the climate change simulations include the forced component T_f. The statistics of T'' in the forced case may differ from those of T' for the equilibrium climate giving rise to in changes in climate variability.

The forced climate change signal is not available by itself but only the combined value $T_0 + T_f + T''$. An estimate of the unperturbed climate mean is available as the average of the control simulation (in the absence of "climate drift") and may be removed to leave $T_f + T''$ or, alternatively the difference between future and past values may be calculated as $\delta T_f + \delta T''$. In both cases the deterministic "signal" T_f is confounded by the random natural variability "noise" T''. The strength of the climate change signal compared to the natural variability noise may be improved by averaging out part of the random natural variability by a combination of ensemble, temporal, and spatial averaging. In what follows, the signal is investigated in terms of global means $\langle X \rangle$, zonal averages $[X]$, and geographical distribution of differences of multiyear averages $\delta \bar{X}$.

## 3 Global mean quantities

3.1 Temperature

The upper panel of Fig. 1 displays the global mean temperature evolution for the period 1900–2100 for the control, the three GHG + aerosol simulations, and the GHG-only simulation, and the lower panel gives the corresponding averages for land and open ocean. As expected, land temperature changes are both larger than ocean values and display more variability. Table 1 summarizes global mean temperature changes for the CCCma coupled model and includes available results from other simulations. Simulated changes from the present (1985–1995) to 2050 range from a low of 1.3 to a high of 1.9 °C with a mean of 1.6 °C for the GHG + aerosol case. The values are reasonably close to one another. The model mean, intermodel standard deviation, and their ratio as an indication of the "signal to noise" ratio are also listed in Table 1. Although this approach is rather simple-minded and involves only four estimates, there is evidence of a reasonably consistent simulated temperature change, at least for the period to 2050. After that time, there are few estimates and the importance of differences in model sensitivity (and other features) are expected to have larger effects and there is less confidence in the projected temperature change for the latter half of the century.

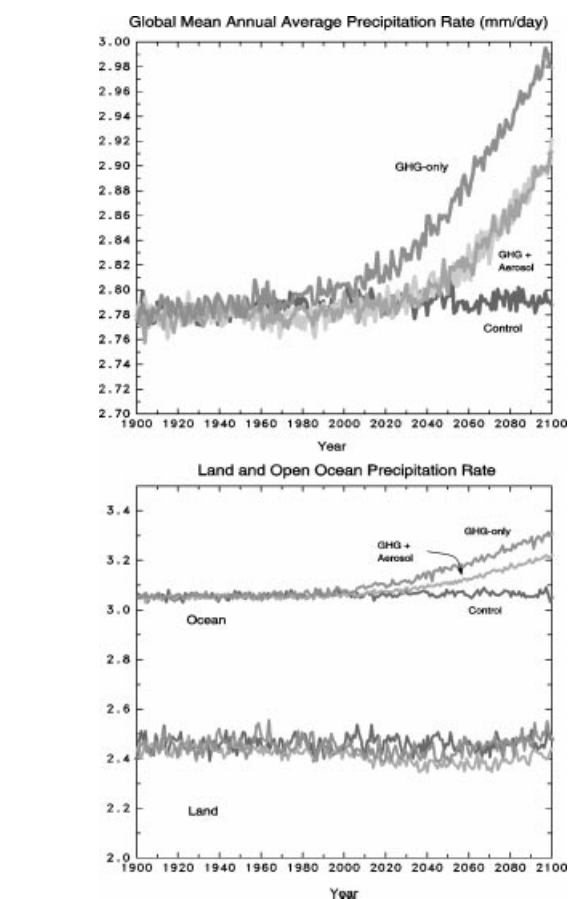### 3.2 Precipitation and evaporation

The evolution of the global average annual mean precipitation (and hence evaporation) rate is shown in Fig. 2 (upper panel) together with the land and open-ocean components (lower panel). The diagrams show:

Table 1 Global mean "climate sensitivity" and simulated temperature changes (°C)

Year	$2 \times CO_2$ sensitivity	GHG + aerosol forcing			GHG only forcing		
	Equilibrium	1900-present	Present-2050	2050–2100	1900-present	Present-2050	2050–2100
CCCma	3.5	0.6	1.7	2.7	0.8	2.4	3.0
GFDL	3.7	0.7	1.9		1.2	2.1	
MPI	2.6	0.5	1.5		0.8	2.1	1.7
UKMO	2.5	0.5	1.3	1.7	0.9	1.7	1.7
Mean	3.1	0.6	1.6		0.9	2.1	
Standard deviation	0.5	0.1	0.2		0.2	0.2	
Signal/noise	5.8	6.9	7.2		5.6	8.3	
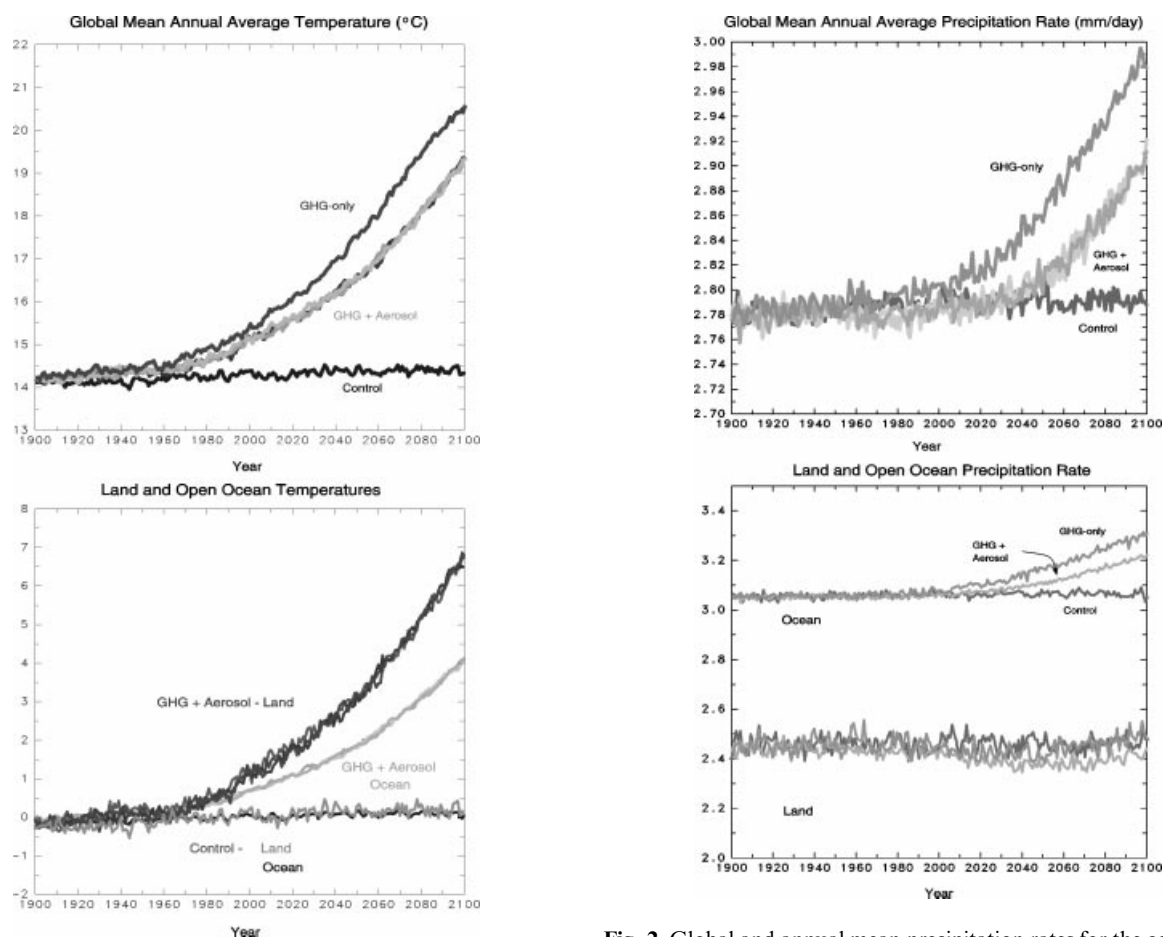
Fig. 1 Global and annual mean temperatures for the control, the three GHG + aerosol simulations and the GHG-only simulations (*upper panel*), and the corresponding temperature changes over land and open ocean (*lower panel*). Units °C

Fig. 2 Global and annual mean precipitation rates for the control, the three separate GHG + aerosol, and the GHG-only simulations (*upper panel*), and the corresponding changes over land and open ocean (*lower panel*). Units mm day^{-1}

(1) the yearly variability of the global mean precipitation rate is larger (compared to the overall change) than that of global mean temperature of Fig. 1; (2) there is the expected overall increase in rate of working of the hydrological cycle as measured by the increase in average precipitation (and evaporation) as the system warms; (3) the GHG-only case and GHG + aerosol cases behave rather differently and the GHG-only curve begins to separate from the control curve considerably earlier than do the curves for the GHG + aerosol cases; (4) the oceanic change in precipitation dominates the global change and the GHG-only case shows an earlier and larger change than the GHG + aerosol average; (5) over land, the precipitation rate for the GHG + aerosol case actually decreases slightly while the GHG-only case recovers toward the end of the period and this foreshadows the changes in surface hydrology discussed below.

3.3 Climate sensitivity and hydrological sensitivity

The difference in the way global precipitation rate increases in the GHG + aerosol and GHG-only cases suggest that the "hydrological sensitivity" of the two cases is different. The climate sensitivity of the real or a model of the climate system is the equilibrium global mean temperature change $\delta\langle T\rangle$ produced by doubling the amount of CO_2 in the atmosphere. The resulting warmer climate is associated with an increase in the rate of working of the hydrological cycle which suggests the associated "hydrological sensitivity" measured by the fractional change in global mean evaporation and precipitation $\delta\langle P\rangle/\langle P\rangle = \delta\langle E\rangle/\langle E\rangle$. The climate sensitivity of models differ as does their hydrological sensitivity and Boer (1993) notes that the proportionality α between these two quantities $\delta\langle P\rangle/\langle P\rangle = \alpha\delta\langle T\rangle$ also differs among models and is not more or less constant, as might be plausible in terms of the Clausius-Clapeyron relationship. The value of α for this version of the AGCM coupled to a mixed layer ocean, is somewhat smaller than that for other models and this can be traced back to the treatment of cloud optical properties and their effect on the surface energy balance.

The evolving climates of the GHG + aerosol and GHG-only simulations suggest a comparison between the time evolving values of temperature and precipitation change. The percentage change in precipitation and the proportionality α between temperature and precipitation change are plotted in Fig. 3. For the mid-century period around 2050, the GHG + aerosol precipitation rate (upper panel) has increased about 1% while the GHG-only precipitation rate increase is closer to 3%. By the end of the century, the GHG + aerosol increase is about 4.5% while that of the GHG-only simulation is near 7.5%. The two lines are not parallel even later in the century implying that the difference is not due only to the difference in the temperature evolution (and the curves could not be scaled with temperature change to bring them into coincidence). The proportionality α (lower panel) is plotted from 1990 to 2100 (the value is not stable for earlier smaller changes) and is clearly not constant but increases with increasing forcing in both cases. Moreover, there is a different relationship between $\delta\langle T\rangle$ and $\delta\langle P\rangle/\langle P\rangle$ in the two cases implying, as argued also in Reader and Boer (1998), that the nature of the forcing affects both the temperature and hydrological sensitivity of the (modelled) system.

3.4 Land hydrology

Basic land hydrology is characterized by the precipitation source, by storage in the form of liquid and frozen soil moisture and snow, and by evaporation and runoff as sinks. The simplest expression of this is $\partial(w + S)/\partial t = P - E - R$ where $w = w_l + w_f$ is the liquid plus frozen soil moisture, S the mass of snow, and P, E, R the rates of precipitation, evaporation and runoff.
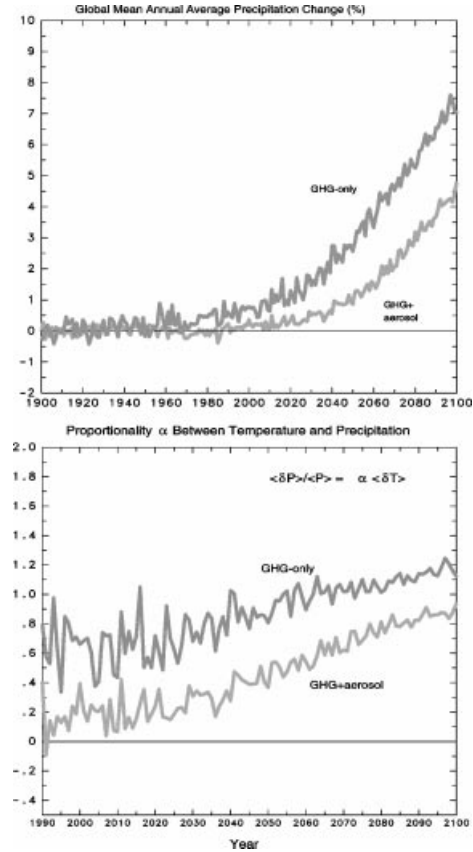

Fig. 3 Global and annual mean precipitation rate changes as a percentage of the 1900–1930 mean value for the average GHG + aerosol and GHG-only cases (*upper panel*), and the proportionality between temperature and hydrological changes as estimated from the GHG + aerosol and GHG-only simulations (*lower panel*)

Soil moisture is usually represented here as a fraction of capacity when it is termed moisture availability. To a first approximation, changes in R are controlled by P and E and the average land surface hydrology is dominated by the Northern Hemisphere land mass.

Some measure of each of the hydrological terms is plotted in Fig. 4 which displays percentage changes compared to the 1900–1930 mean for the control, average GHG + aerosol, and GHG-only simulations. Decadal means are plotted in order to delineate the long time scale evolution of these quantities and they are labelled with the last year in the decade. The scales are different for the different variables. The curves for the GHG + aerosol and GHG simulations begin to separate appreciably from the control values only in the twenty-first century.

Precipitation decreases over land in both seasons and for both GHG + aerosol and GHG-only cases but it recovers and begins to increase again towards the end of the simulation in DJF but not in JJA. Evaporation behaves similarly for DJF but generally increases in JJA in association with the warmer northern summer temperatures. $P - E$ and soil moisture availability show modest decreases in DJF but large percentage decreases in JJA

DJF Land Surface Hydrology

Fig. 4a, b Changes in land surface hydrology components as a percentage of the 1900–1930 means for DJF and JJA. Decadal means are plotted and values are labelled by the last year in the decade
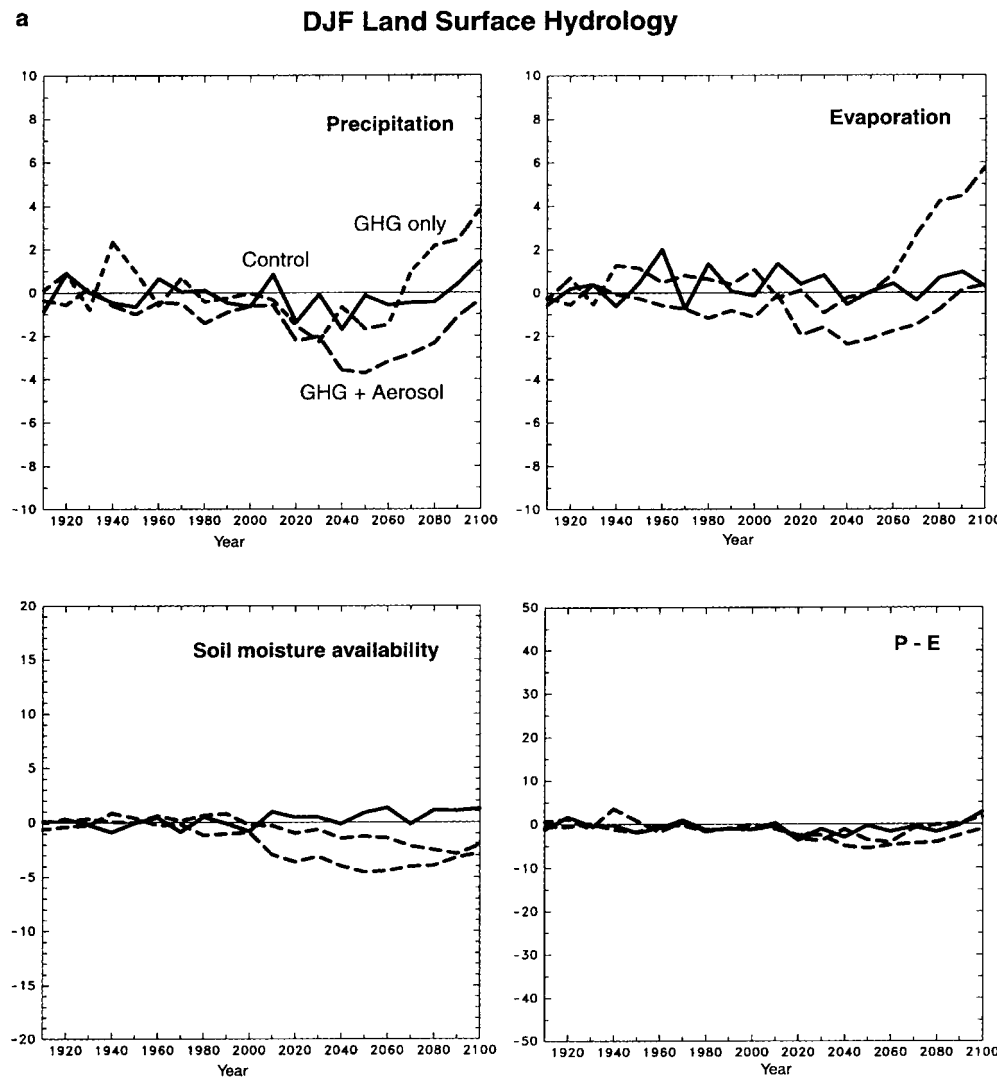
indicating a marked drying tendency in northern sum-
mer. The differential effect of the aerosol forcing is to
decrease both precipitation and evaporation and to in-
crease soil moisture availability.

3.5 Cryosphere

The evolution of snow cover over Northern Hemisphere
land and of sea-ice area in both hemispheres for the DJF
and JJA seasons is displayed in Fig. 5. These are decadal
averages of the area with snow amounts greater than
3 cm accumulation and sea-ice thickness greater than
5 cm. Snow cover amounts are reasonable for the con-
trol simulation. Snow cover is relatively stable from 1900
to the present but then begins an accelerated decrease
in both the GHG + aerosol and the GHG-only cases.
Northern Hemisphere snow cover decreases by about
50% by the end of the simulation for DJF and almost
disappears in JJA. The differential effect of the aerosol
forcing is to moderate this decrease as expected. The
Northern Hemisphere sea-ice area simulated for the

control case is somewhat smaller than that observed and
there is a slight decreasing trend. Once again, however,
there are only minor changes simulated to occur from
1900 to the present after which a pronounced retreat of
the ice for both GHG + aerosol and GHG-only simu-
lations begins whereby the northern ice cover virtually
disappears by the end of the simulation. The effect of the
aerosols is again to moderate this decrease. The South-
ern Hemisphere decrease in ice cover is considerably less
marked as is the differential effect of the aerosol forcing.
The control simulation also displays sufficient long-term
variability so that the JJA control run ice area curve
does not separate from the GHG + aerosol and GHG-
only curves until late the twenty-first century.

4 Latitudinal structures

4.1 Temperature

The difference of the zonally averaged temperature from
the average of the control simulation is shown in Fig. 6

b   **JJA Land Surface Hydrology**
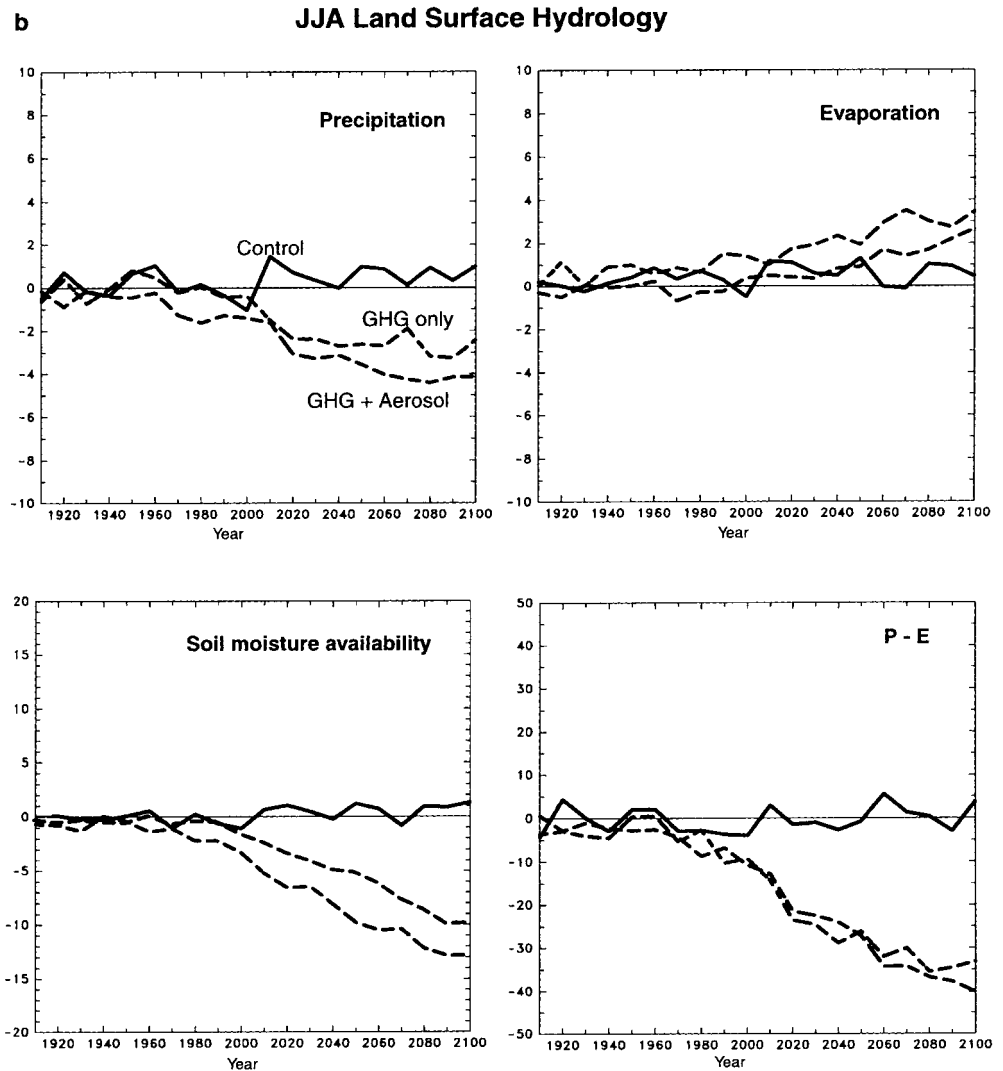
for the average of the three GHG + aerosol simulations $\delta[\bar{T}]$, the GHG-only case $\delta[T_g]$. An estimate of the aerosol effect is obtained as the difference $\delta[T_a] = \delta[T_g] - \delta[\bar{T}]$. From the diagram: (1) there is a modest simulated climate warming to the present for the GHG + aerosol case; (2) the warming accelerates markedly beyond the turn of the century based on this forcing scenario; (3) the warming amplifies with latitude in the Northern Hemisphere but there is a marked asymmetry between the warming of the two hemispheres; (4) the effect of the aerosols to retard the warming with the largest cooling at higher latitudes rather than at the latitude of maximum aerosol forcing. The hemispheric asymmetry of warming is a feature of coupled model simulations (IPCC 95) although not usually presented in the form of Fig. 6 nor available for the GHG + aerosol forcing scenario used here. Earlier simulations of Manabe et al. (1991) and Cai and Gordon (1998) forced with increasing CO_2 concentrations, for instance, show similar but my no means identical patterns to those shown in Fig. 6. The considerable

warming toward the end of the period corresponds to a $4 \times CO_2$ increase from the control climate partially offset by the negative aerosol forcing.

Reader and Boer (1998) note that in the case of equilibrium climate change calculated with this AGCM coupled to a mixed layer ocean, the general effect of the aerosols is to offset the globally distributed GHG warming pattern rather than to strongly counteract the warming in the region where the negative aerosol forcing is largest. This can be quantified also in the case of the transient zonally averaged temperature change (dropping the brackets) as $\delta T_a = \delta T_{NL} + \delta T_L = a\delta T_g + \delta T_L$ where the temperature difference associated with the aerosols is decomposed into a component associated with a distributed or non-local response and the remainder considered the local response. The non-local response is taken to be a simple scaling of the non-local GHG-only temperature pattern of Fig. 6. The value of the regression factor a is obtained by least-squares under time and zonal averaging and the result of the decomposition is shown in Fig. 7. The associated squared

a
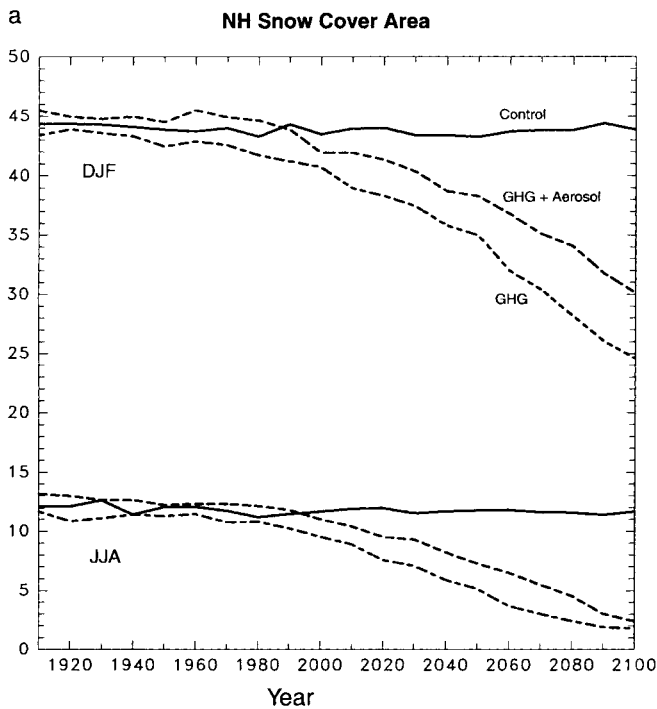
Fig. 5 **a** Northern Hemisphere area of snow cover amounts greater than 3 cm for DJF and JJA; and **b** Northern and Southern Hemisphere areas of sea-ice thicknesses greater than 5 cm. Units 10^{12} m^2

correlation coefficient of 91% measures the variance of the net aerosol response pattern (top panel) that can be explained in the usual statistical sense by scaling the GHG-only pattern (middle panel). The remaining local pattern (bottom panel) shows only a weak Northern Hemisphere local response to aerosol forcing. This result supports the contention that the response to localized forcing is not itself localized but is "globalized" with feedbacks amplifying (and suppressing) the response in regions removed from the direct effect of the forcing.

The evolution of the non-zonal component or standing eddy structure of the temperature field $\delta T^* = \delta T - \delta[T]$ is measured by the spatial variance $[\delta T^{*2}]$. Figure 8 displays the standard deviations $[\delta \bar{T}^{*2}]^{1/2}$ for the average of the GHG + aerosol cases. The effect of the aerosols, calculated from $[\delta T_a^{*2}] = [\delta \bar{T}^{*2}] - [\delta T_g^{*2}]$, (not shown) indicates a *reduction* of standing eddy variance due to aerosols. The diagram indicates that: (1) associated with the increase in zonally averaged temperatures $[T]$ there is a corresponding increase in the deviations T^* about the zonal average; (2) there is only a very modest increase to the present but the rate of increase accelerates in the next century; and (3) there is an asymmetry between the hemispheres and an amplification with latitude in the Northern Hemisphere. In this, the general evolution of the standing eddy variance is broadly similar to the zonal mean temperature itself. In other words, the standing eddies or zonal asymmetries in the temperature field amplify as the temperature increases. This is asso-

ciated primarily with the increasing land-sea temperature contrast indicated in Fig. 1.

The amplification of the standing eddy temperature structure with increasing GHG forcing is partially counteracted by the aerosol forcing. This is not an obvious consequence since the aerosol forcing (Fig. 5 of BFRR) itself has non-zonal structure while the GHG-only forcing has little zonal structure, so that the aerosol forcing might be expected to enhance rather than suppress the standing eddies. However, the dominant part of the aerosol response, as noted already, acts to counteract the overall GHG warming pattern and so to decrease zonal asymmetries in temperature.

4.2 Precipitation and evaporation

The global hydrological cycle becomes more vigorous under evolving anthropogenic forcing. The changes are not uniform over land and ocean nor with latitude, however. Since precipitation and evaporation are (generally) positive quantities, changes are usefully presented as percentages of the average control run values at each latitude.

Zonally averaged distributions of percentage precipitation and evaporation changes are shown in Figs. 9 and 10 and indicate latitudes of both increasing and decreasing values. Pentadal averages are plotted in order to smooth out some of the variability of these quantities, especially for precipitation. The diagrams indicate that the patterns begin to organize themselves, visually at least, at about the current time. The overall asymmetry between hemispheres, noted for temperature, is mirrored in evaporation as would be expected from the dependence of the saturated vapour pressure with temperature and its effect on evaporation. Evaporation decreases occur in a band over the southern ocean towards the end of the period despite weak (average) warming and a slight increase of wind speed implied by the change in the pressure gradient of Fig. 19. The implication is that the decrease in evaporation is a consequence of a more stable low level temperature structure (Fig. 13) which acts to decrease evaporation. Evaporation is comparatively small in this region and it is not clear if this reduction is a common feature of other climate change simulations. The largest increases are found in polar regions in association with the decrease of sea-ice.

Changes in precipitation are not often displayed in percentage terms although the practical importance depends less on the absolute value than on the relative change compared to the current climatology. There are alternating bands of increase and decrease in precipitation associated with changes in both the position and magnitude of the precipitation distribution. The hemispheric asymmetry in precipitation change is much less striking than that for temperature and evaporation. Maximum percentage increases are found in polar regions where precipitation is low and the increase is apparently a common simulation result (IPCC 95)

b   **Sea-Ice Area**
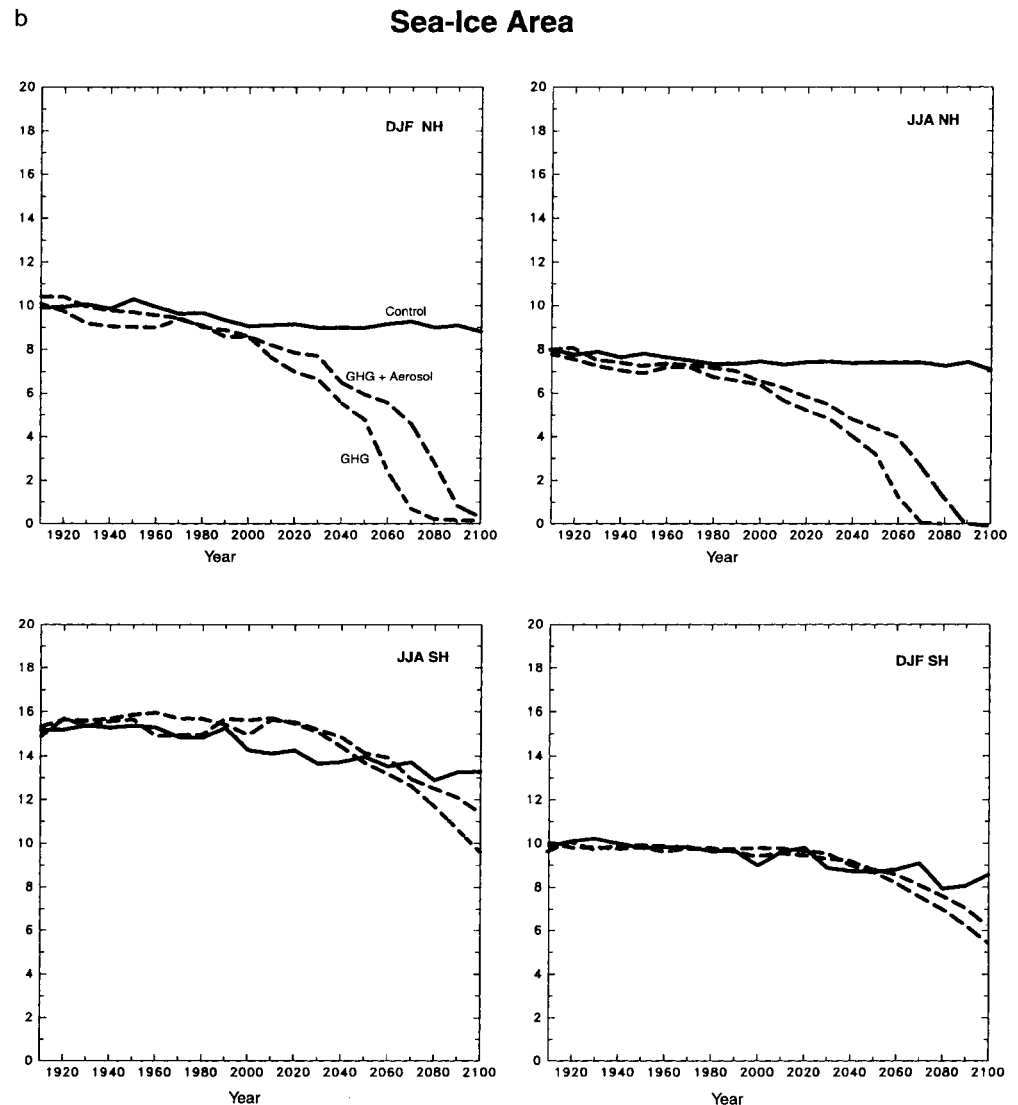
although not expressed in this way. Poleward transports of moisture generally increase in the warmer climate despite a reduction in the meridional circulations and the eddies as a consequence of increased moisture content in the warmer atmosphere (e.g. Boer 1995). Minimum percent increases, or even slight decreases, in precipitation are found at the latitudes of the subtropical highs.

The effect of the aerosols is to moderate or decrease the changes in both precipitation and evaporation as expected. While the largest effects are in the polar regions of maximum percentage precipitation and evaporation change, there is some suggestion of a direct aerosol effect on precipitation at the northern hemisphere middle latitudes of aerosol forcing.

4.3 Soil moisture

Figure 11 gives zonally averaged percentage changes in soil moisture availability to reflect that the practical

importance of the change relative to the current climatology. Decadal mean changes are plotted for DJF and JJA for the average of the three GHG + aerosol simulations together with the inferred effect of the aerosols (the GHG-only change is then the sum of the two). The region covered is from 30°S to 70°N so as to avoid latitudes with little or no land. The soil moisture parametrization in the model is relatively unsophisticated but attempts to incorporate some effects of vegetation and soil type in terms of geographically varying evapotranspiration factors and soil moisture storage capacity (McFarlane et al. 1992). The model soil moisture integrates the overall inputs and outputs of the land hydrology and provides an indication of the expected change. In common with most models (for GHG-only forcing in IPCC 1995), soil moisture increases in high northern latitudes in winter where the increase in precipitation outweighs the increase in evaporation. Soil moisture generally decreases in northern summer and in both seasons in the southern hemisphere. Evaporation changes little on the zonal average in these cases and the

Surface air temperature change

Average GHG + Aerosol

GHG only

### Estimated aerosol effect
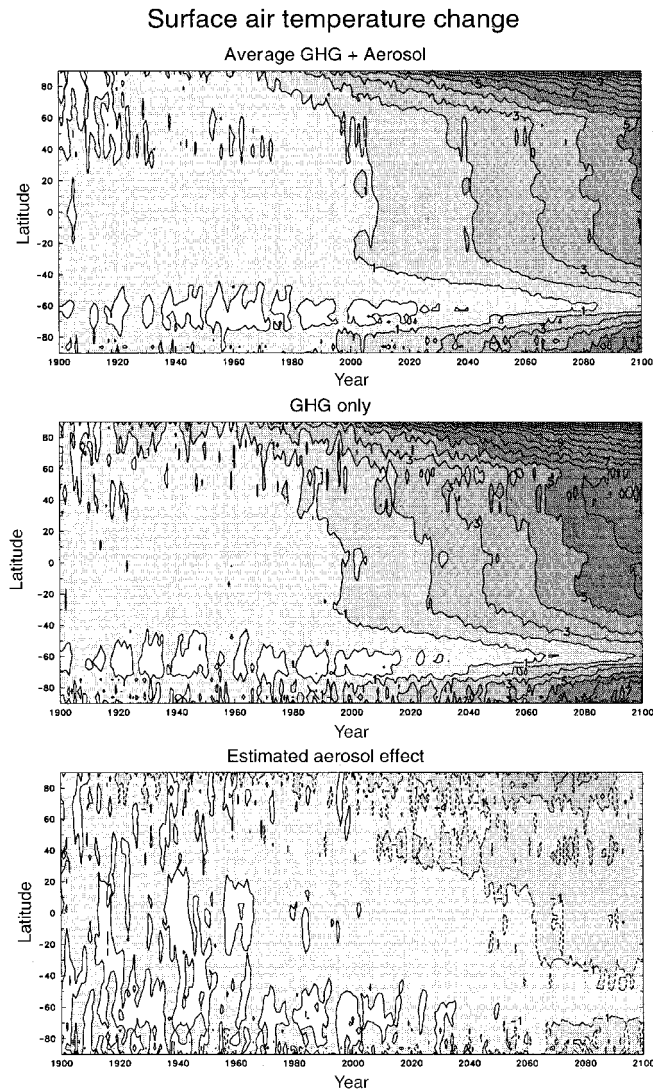
Fig. 6 Zonally averaged surface air temperature changes for the average GHG + aerosol and GHG-only cases and their difference as an estimate of the effect of the aerosol forcing. Units °C

decrease in soil moisture is a consequence of decrease precipitation and an increase of runoff. The effect of the aerosol forcing is generally to increase soil moisture (i.e. to reduce the drying tendency compared to the GHG-only case) as expected.

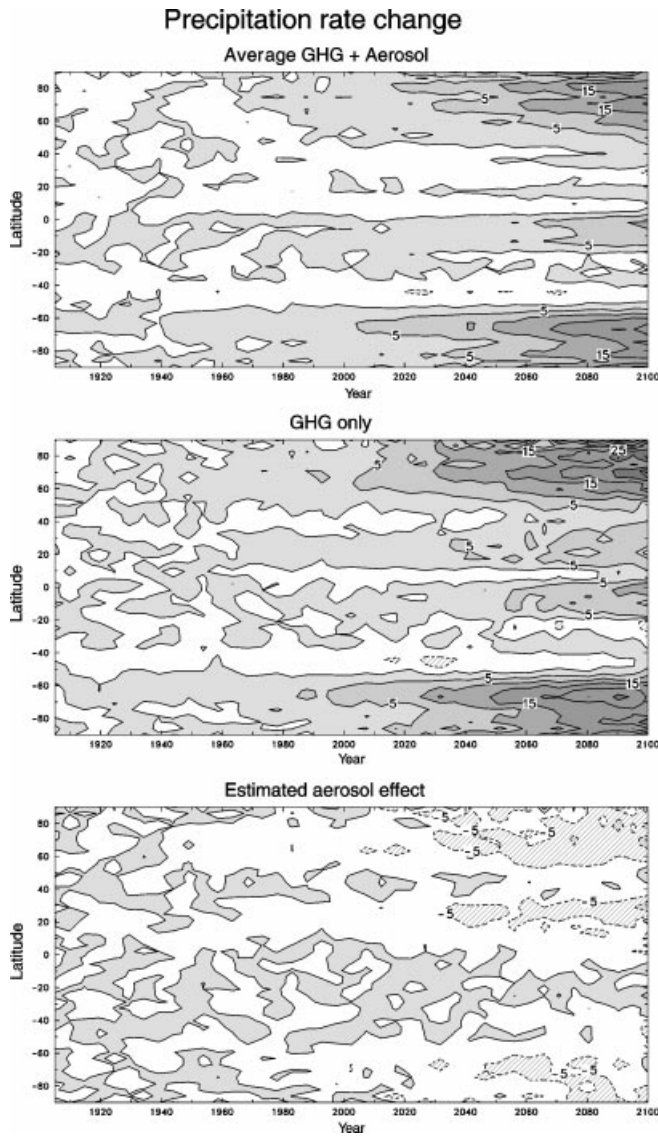## 5 Cross sections and geographic structures

The ultimate aim of CGCMs is to simulate the three-dimensional evolution of climate but the amount of data produced is enormous. The evolution with time of zero- and one-dimensional quantities, such as the global and zonal averages, can be displayed relatively straightfor-wardly as is done in previous sections. A display of the temporal evolution of two- or three-dimensional fields is more difficult and treated here by calculating differences for selected 20-year average "time-slices".

Temperature response to the aerosol

Net response

Non-local response
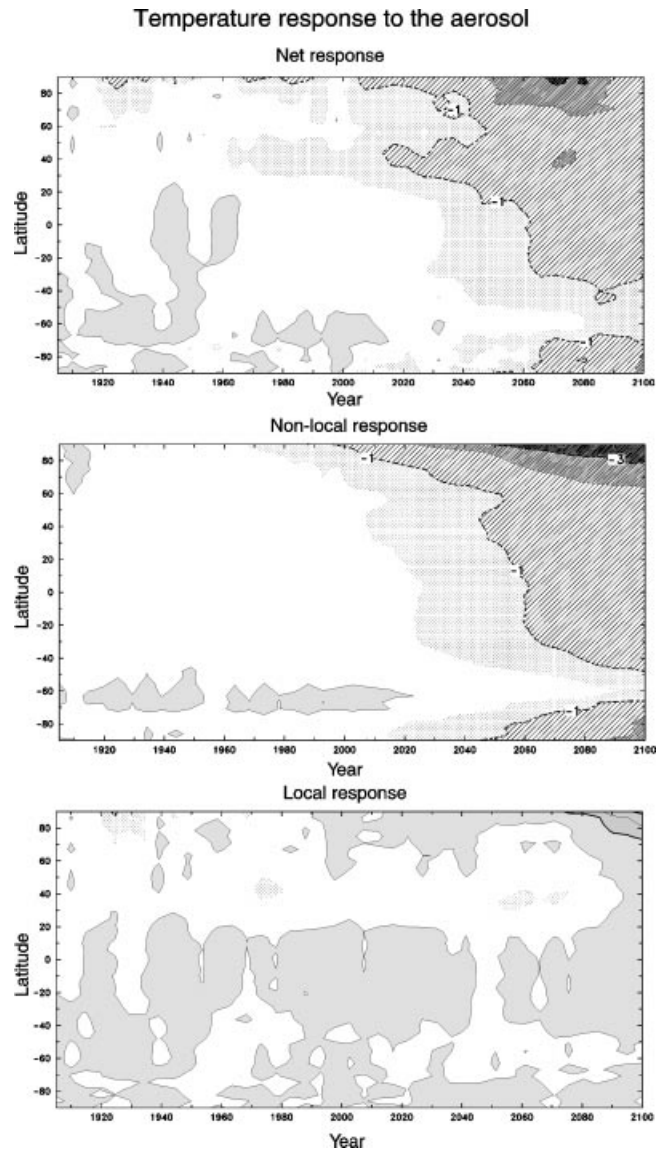
Local response

Fig. 7 The temperature response to aerosol forcing: estimated net response (*upper panel*), the "non-local" response obtained by scaling the GHG-only response (*middle panel*) and the "local" response to aerosol forcing (*lower panel*). Units °C

Standing eddy temperature structures

Average GHG + Aerosol
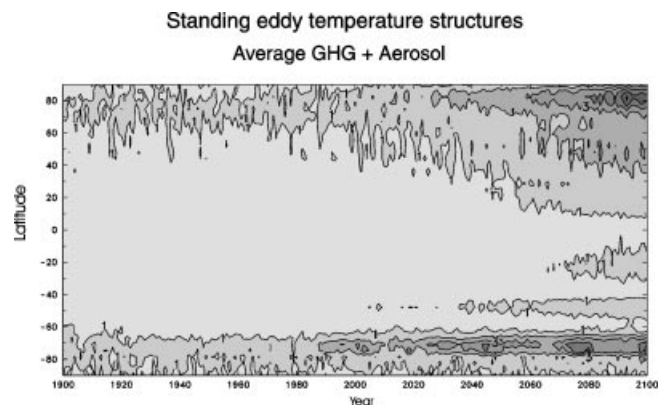
Fig. 8 The change in the zonal asymmetry or standing eddy structure of the temperature for the GHG + aerosol simulation. Units °C

Precipitation rate change

Average GHG + Aerosol

GHG only

Estimated aerosol effect

Evaporation rate change

Average GHG + Aerosol

GHG only

Estimated aerosol effect

Fig. 9 Zonal structure of precipitation rate change as a percentage of the control run average for the average GHG + aerosol and GHG-only cases with their difference indicating the effect of the aerosol forcing
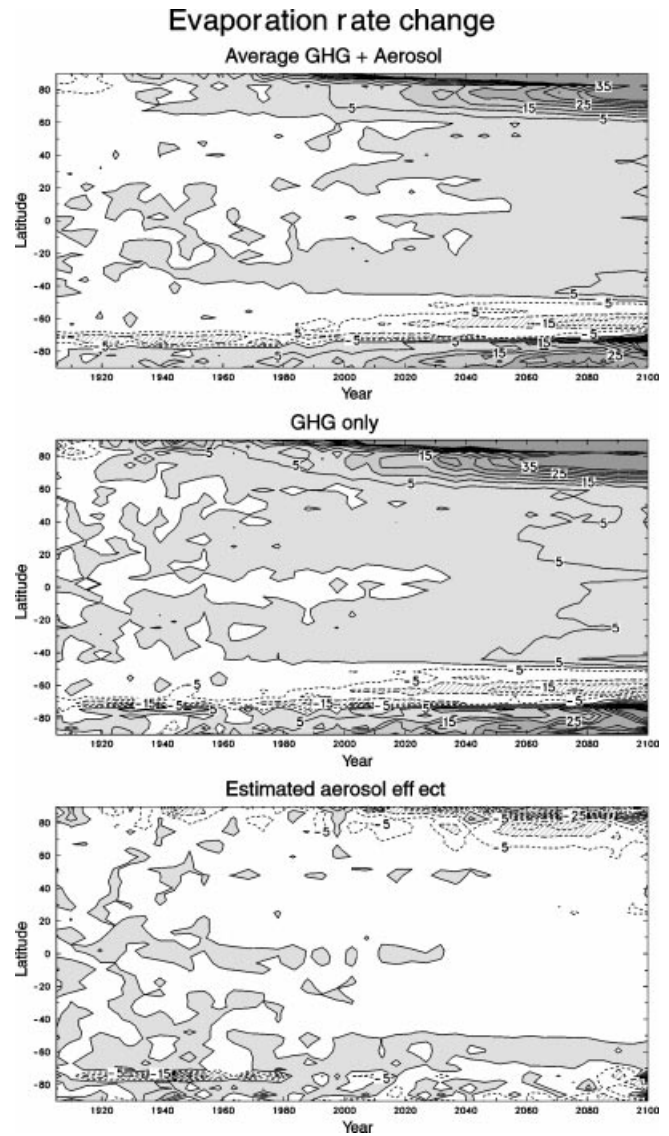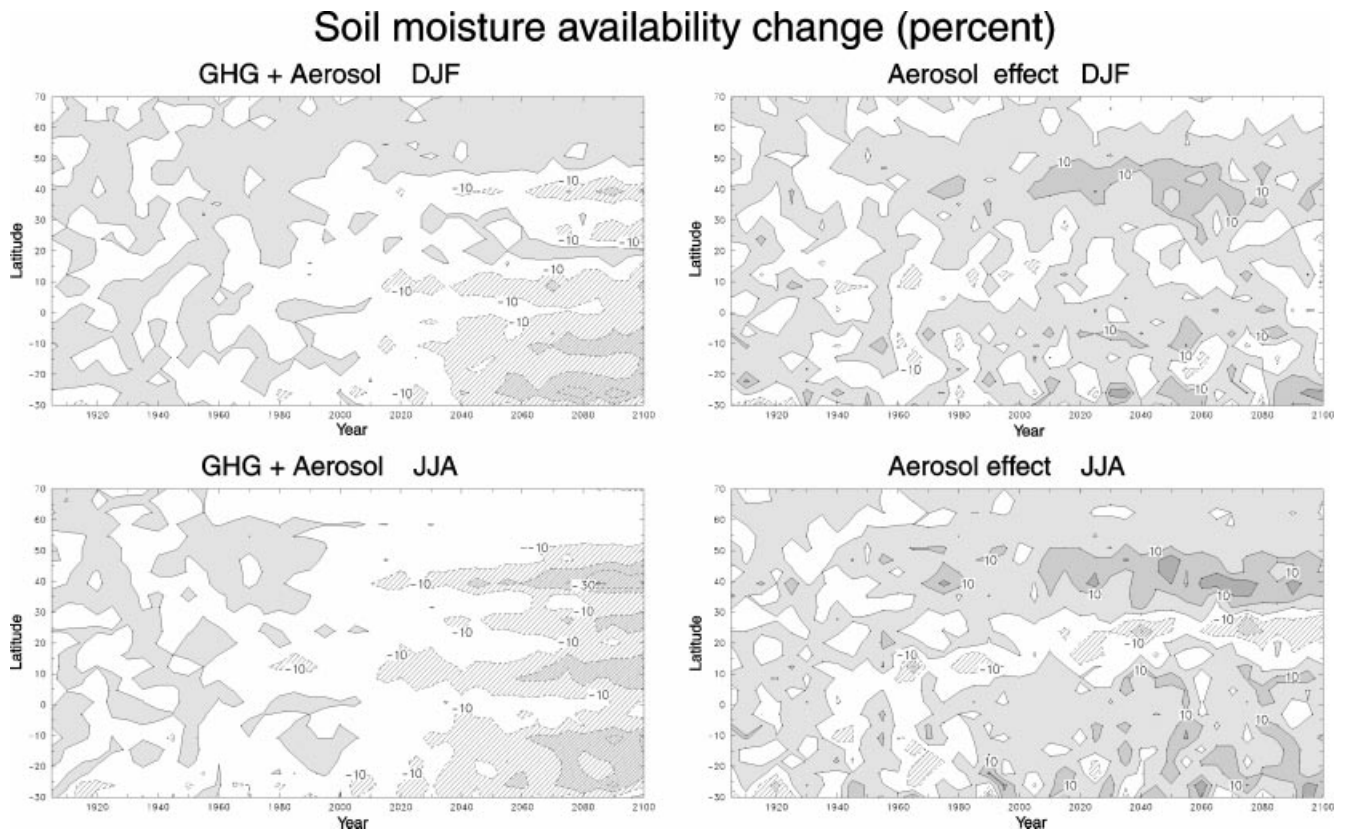
Fig. 10 Zonal structure of evaporation rate change as a percentage of the control run average for the average GHG + aerosol and GHG-only cases with their difference indicating the effect of the aerosol forcing

5.1 Signal evolution

The evolution of the climate change "signal" versus the natural variability "noise" is studied in a statistical context by the use of the t-statistic $t = (\bar{Y} - \bar{X})/S$ at points over the globe for several variables of interest. The statistical calculations follow Crow et al. (1960) and von Storch and Zwiers (1999) where $\bar{Y}$ and $\bar{X}$ are 20-year means from the GHG + aerosol and control simulations and S is the estimate of the pooled standard deviation (which automatically takes into account the different sampling variability of the average GHG + aerosol and GHG-only means). A modification of the test to approximately account for serial correlation in the data is discussed in the Appendix of

Boer et al. (2000). The 20-year DJF and JJA means from the average GHG + aerosol simulation are compared with the corresponding 20-year means from the control simulation. Similarly the GHG + aerosol and GHG-only simulations are compared with one another to indicate the evolution of the aerosol signal.

Figure 12 shows the fractional area of the globe (or of the land surface for soil moisture) for which non-overlapping 20-year means of surface air temperature, mean sea-level pressure, precipitation and soil moisture (the values are labelled with the final year of the 20-year average period) are judged to be significantly different at the nominal 5% level. Spatial correlation in the fields means that the test does not perform at its nominal significance level. It does, however, provide an indication of the evolution of the climate change signal which

Soil moisture availability change (percent)

Fig. 11 Zonal structure of soil moisture availability change over land as a percentage of the control run average for the average GHG + aerosol and the difference with the GHG-only cases indicating the effect of the aerosol forcing

is the intent of the diagram. The upper panels of the figure show that: (1) the surface air temperature signal is by far the most robust both for the change with respect to the control simulation but also for the difference between the GHG + aerosol and GHG-only cases; (2) the signals in mean sea level pressure, soil moisture, and precipitation are weaker than that for temperature and only begin to increase appreciably after the turn of the century; (3) presumably because of its larger spatial scales, mean sea-level pressure shows a signal intermediate between temperature and the moisture related precipitation and soil moisture variables; and (4) the differences in signal between DJF and JJA, measured in this way, are modest.

The effect of the forcing associated with aerosols is given in the lower panels of Fig. 12 based on the difference between the GHG + aerosol and GHG-only cases. The aerosol signal in temperature is weaker and is delayed compared to the combined GHG + aerosol signal shown in the upper panels. The aerosol effect on precipitation and soil moisture is comparatively weak, especially in DJF, and overall is slightly greater in JJA as is consistent with the stronger aerosol forcing in that season.

Figure 12 serves to give a broad indication of the overall significance of the difference maps presented in

subsequent sections. The simulated changes in all variables are certainly marked in the latter part of the period as indicated in the upper panel of the figure.

## 5.2 Temperature cross sections

Latitude-height cross sections and maps of the geographical distribution of temperature and other fields are displayed as differences between the 20-year averages for the years 1975–95, 2040–60 and 2080–2100. Figure 13 displays cross sections of annual average zonal temperature change for the average of the three GHG + aerosol simulations as well as the effect of the aerosol in counteracting the warming. The DJF and JJA cross sections (not shown) are remarkably similar to this annual average, although the northern polar region of surface warmth is magnified in the winter season. The diagrams indicate: (1) that maximum temperature changes to 2040–60 are cooling in the stratosphere but to 2080–2100 they are warming in the tropical upper troposphere; (2) the warming pattern resembles that for the $2 \times CO_2$ equilibrium calculation of Boer et al. (1992) away from the surface; and (3) near the surface there is an asymmetry in the warming, and a difference from the equilibrium calculation, with the Northern Hemisphere middle and high latitudes warming more than the corresponding Southern Hemisphere regions. This latter feature is characteristic of fully coupled models compared to those with mixed layer ocean components (IPCC1995).

Fraction of area for which variable judged "significantly" different

between GHG+aerosol and Control simulations
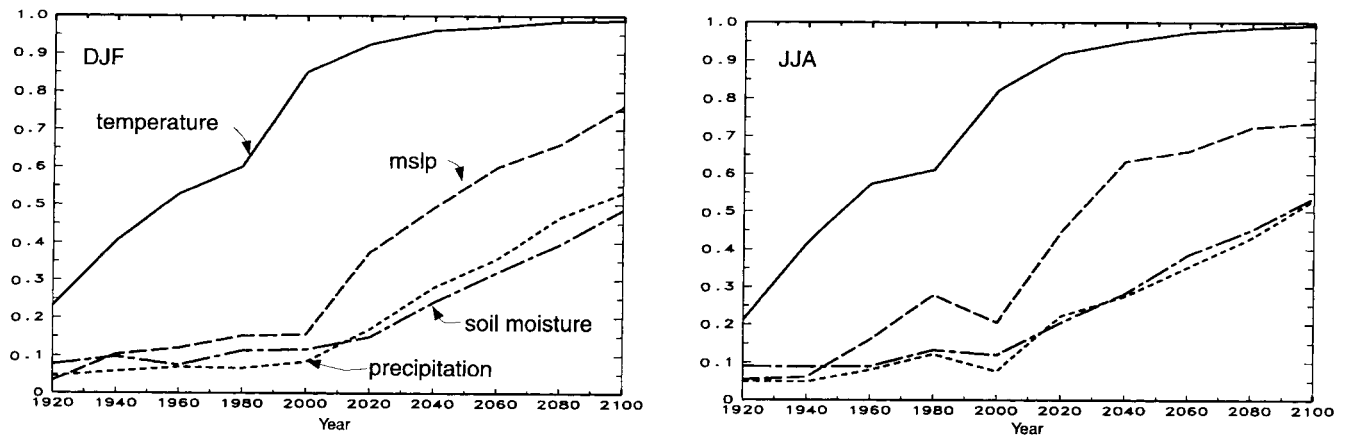
between GHG and GHG+aerosol simulations
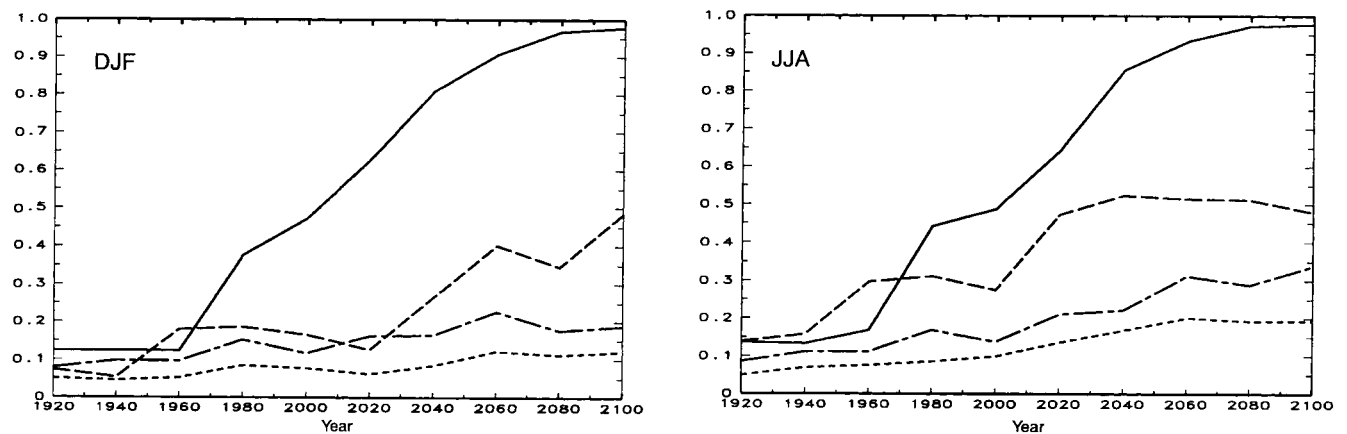
Fig. 12 Fraction of the globe for which the 20-year means of each quantity are judged to be "significantly different" from one another as measured by the local t-test at the nominal 5% significance level. The values are labelled by the final year in each 20-year period

The direct radiative effect of the aerosol is to reflect a fraction of the incoming solar radiation at the surface and hence to act directly to cool the surface. The aerosol is found mainly in the Northern Hemisphere subtropical and middle latitudes. Nevertheless, the net effect of the aerosol is preferential cooling in the upper tropical troposphere indicating once again that the feedbacks in the system determine the nature of the climate response to a change in forcing rather than the distribution of the forcing itself. The aerosol affects the tropospheric energy budget by interfering with the surface energy balance but the effect is redistributed by the same feedback processes that act to warm the atmosphere when the perturbation is a positive one. The importance of the surface energy balance in mediating the warming (or cooling) is also supported by the relative lack of an aerosol effect in the stratosphere where the cooling is a direct radiative effect of the GHG concentration.

Figure 14 displays corresponding cross-sections of annual average zonal temperature change for the ocean

for the first of the GHG + aerosol simulations. Results are similar for the other cases. Here values are masked out if less than 10% of the grid points around the latitude circle are ocean. The simulated warming is largely confined to the upper part of the ocean and this is especially the case in the tropical region. At higher latitudes the warming penetrates deeper as a consequence of increased interaction between surface and deeper waters but the nature of this penetration is different in the two hemispheres. In the Northern Hemisphere the warming decreases more or less monotonically with depth, in contrast to southern high latitudes where the maximum warming is found beneath the surface layers. The comparatively small warming (or even local cooling) seen at high southern latitudes over the ocean (see Fig. 15) is one consequence of the sequestering of heat in this way.

5.3 Surface air temperature

The associated surface air temperature changes are displayed in Fig. 15 for the DJF and JJA seasons. These may be contrasted with the corresponding equilibrium calculations in Boer et al. (1992) (Fig. 5), compared with the relatively few GHG + aerosol simulations avail-
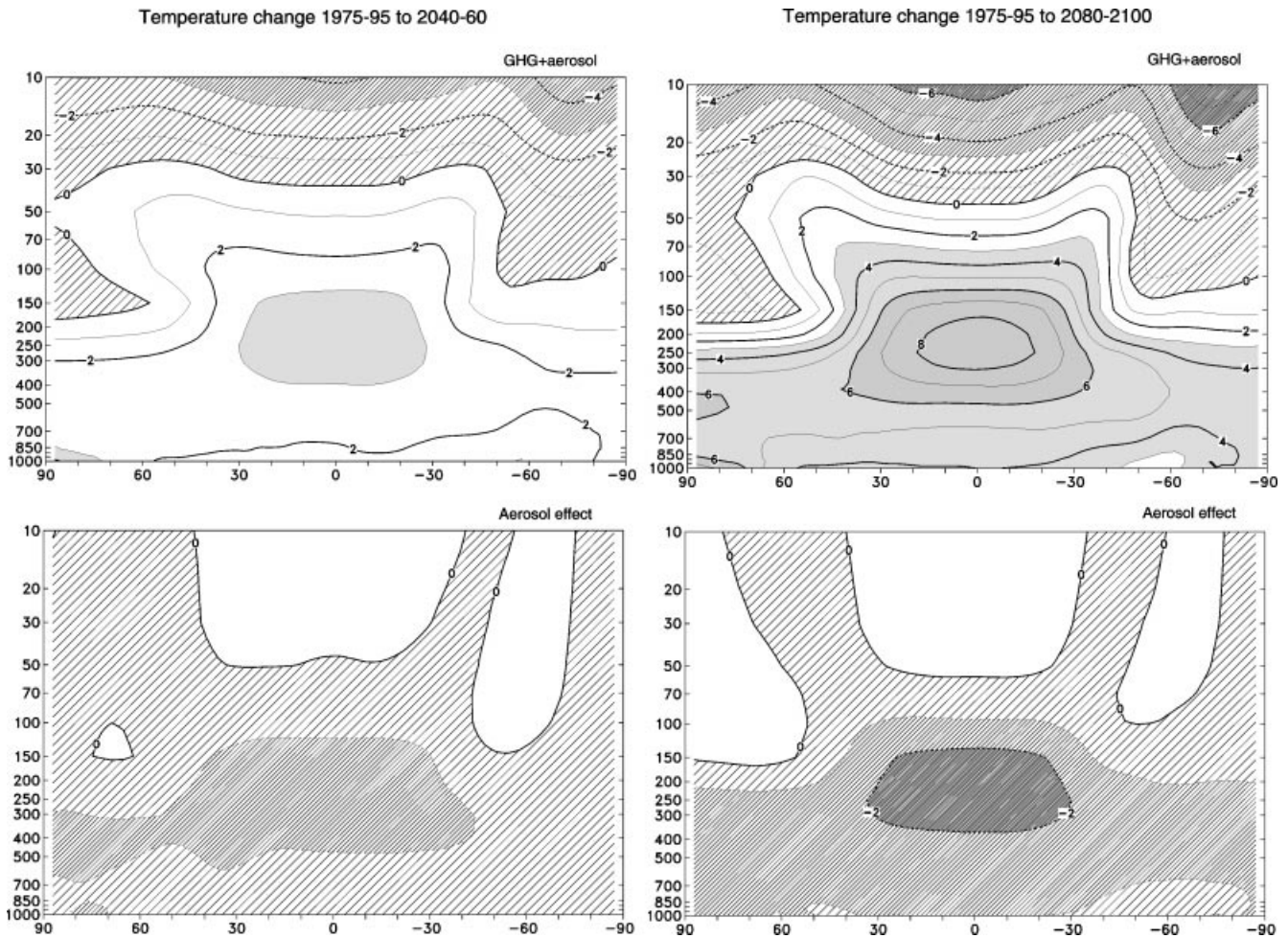
Fig. 13 Zonal cross sections of annual mean temperature differences from the 1975–95 period to 2040–2060 and 2080–2100 for the average of the GHG + aerosol simulations and the effect of aerosol forcing. Units °C

able, and with the more common 1% per year increasing CO_2 simulations described for instance in IPCC1995. Some features are: (1) asymmetric warming with regions of retarded warming or even slight cooling in the Southern Ocean; (2) secondary regions of retarded warming or slight cooling near Greenland in the north Atlantic and the India/Indochina region over land; (3) enhanced warming over the continents and especially the northern land and ice during DJF where, for the later period, there is little sea-ice; (4) enhanced warmth in the tropical eastern Pacific, which might be termed "El Nino-like", a feature of the coupled model response which is absent in the equilibrium mixed-layer ocean case.

Most of the broad features of the surface temperature response bear a qualitative resemblance to recent coupled model simulations but there is considerable quantitative scatter among results. For instance, the "El Nino-like" SST response, which depends on ocean dynamics in this model, has been found only in some other

coupled simulations (IPCC1995; Meehl and Washington 1996) and with differing amplitude. Intermodel differences may arise due to somewhat different forcing prescriptions but are presumably mainly due to a combination of differing model sensitivity (or put in another way, differing model error) together with a contribution from natural variability (as discussed in Sect. 2). The comparison of observed and simulated temperature trends discussed in BFRR gives some indication that the model is responding appropriately to imposed GHG + aerosol forcing changes during the twentieth century. However, the response to the strong projected increase in forcing in the twenty-first century is expected to depend more critically on model sensitivity than does the twentieth century temperature change (e.g. Sect. 4.3 in BFRR) and so are uncertain in this respect.

Figure 16 gives the aerosol effect on the annual average temperature obtained as the difference between the GHG-only and the GHG + aerosol simulations for the two periods. As has been stressed previously and in Reader and Boer (1998), the aerosol effect is seen as a distributed pattern of cooling which tends to counteract the overall warming pattern and only secondarily to reflect the more or less local nature of the aerosol forcing.

Temperature changes in the ocean
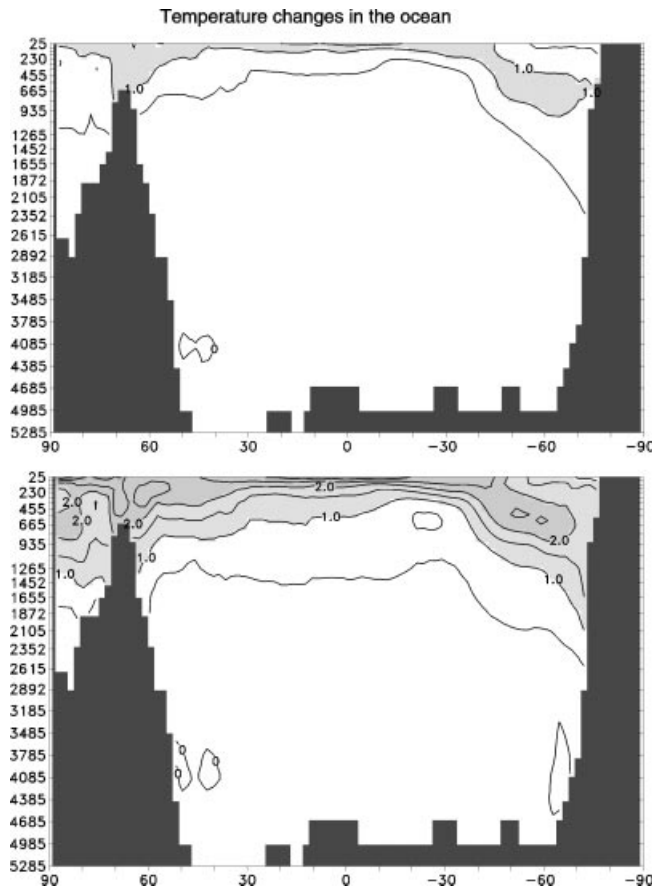
Fig. 14 Zonal cross sections of temperature change for the ocean from the present to 2040–50 (upper) and 2080–90 (lower) for GHG + aerosol forcing. Units °C

5.4 Precipitation

The geographical distribution of the change in precipitation is displayed in Fig. 17. The percentage change is again given as being more indicative of the local importance of the simulated changes than the change in precipitation amount itself. While the overall trend is for an increase in precipitation with time as shown in the global and zonally averaged values of Figs. 2 and 10, there are nevertheless local structures involving both increases and decreases. The figure indicates: (1) an El Nino-like signal in precipitation in the tropical Pacific with decreases in precipitation in the west and increases in precipitation in the central and eastern Pacific and on the western coast of North America; (2) general increases in precipitation in middle and high northern latitudes in DJF including an apparent shift in the rain band across Africa; (3) decreases in DJF precipitation on the eastern sides of the continents in the North America and India/China areas; (4) decreases in precipitation over large portions of the northern continents in JJA as well as decreases over low-latitude Southern Hemisphere land regions and adjacent oceans: and (5) increases in DJF and reductions in JJA precipitation for and to the west of Australia.

Figure 12 indicates that the climate change signal in precipitation is not as distinct as that for more robust variables like temperature and this is seen also in the twentieth century analysis in BFRR. The strong (percentage) changes of precipitation simulated in the Pacific are not a feature of models without an El Nino-like mean response while other broad features such as the increase in precipitation at higher latitudes are common. IPCC1995 reports that an increase in the India/southeast Asia region is a reasonably common feature of model simulations which is seen here only for the late twenty-first century in JJA.
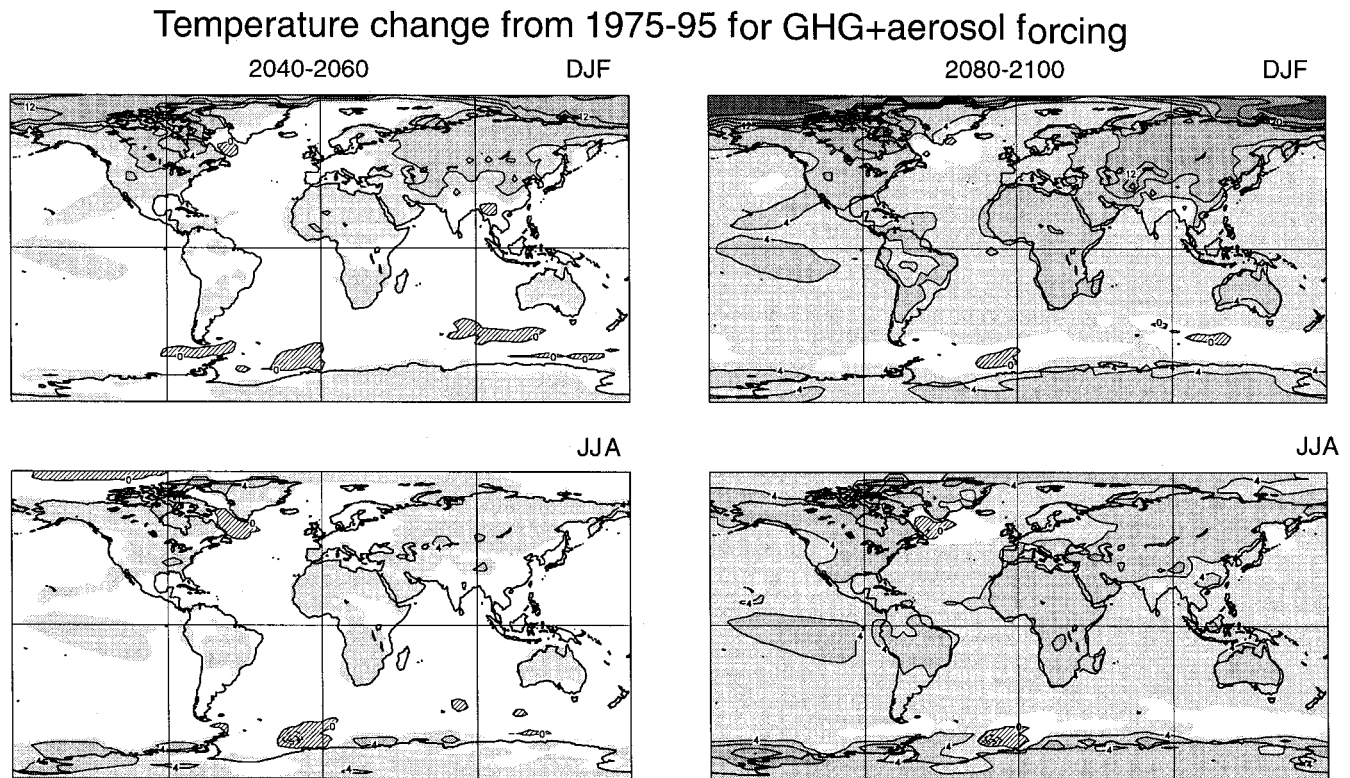
Figure 12 also indicates that the effect of the aerosol forcing on precipitation change is weak. The pattern of change (not shown) is relatively poorly organized over much of the globe although there are some regions of large change such as the Indian region in JJA. The broad effect of the aerosols is to weaken the precipitation change patterns of Fig. 17 in association with the reduced forcing.

5.5 Soil moisture

Soil moisture and precipitation changes share a common "signal strength" according to the upper panels of Fig. 12. As for precipitation, soil moisture is an inherently positive quantity and percentage changes are presented in Fig. 18 as representing the local importance of the change more clearly than would absolute amounts. Recall that the soil moisture capacity varies with location in the model. Latitude dependent features of the soil moisture change are discussed in Sect. 4 in connection with the broad changes in precipitation and moisture transport. The geographical pattern of soil moisture change shows a general decrease in tropical regions and in the summer hemisphere consistent with the expected increase in evaporation in the warmer climate as well as a decrease in precipitation in this season. There are, nevertheless, regions which do not follow this tendency including the Indian region where soil moisture tends to increase and the southern USA where soil moisture increases on the west and decreases on the eastern sides of the country.

There is some tendency for increased soil moisture at high latitudes in winter. Both of these aspects are qualitatively similar to the results discussed in IPCC 1995, for instance, but the comparison of results is hampered by different treatments of soil moisture among models as well as lack of qualitative agreement. As by now expected, the general effect of the aerosols is to counteract the GHG-forced pattern and this is the case also for soil moisture. Figure 12 shows that the aerosol signal in soil moisture is modest overall. Aerosols act to decrease soil moisture availability over some middle and high northern latitudes with largest decreases in the land surrounding the Indian Ocean and Arabian Sea as well as on the western coast of North America.

Temperature change from 1975-95 for GHG+aerosol forcing

2040-2060   DJF   2080-2100   DJF
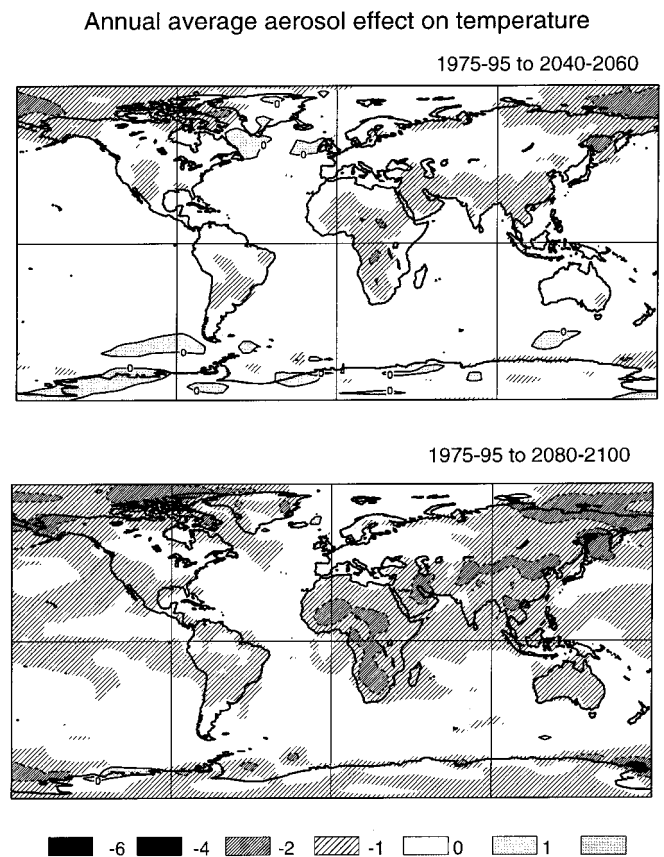
JJA   JJA

Fig. 15 Differences in DJF and JJA temperatures from 1975–95 to 2040–2060 and 2080–2100 for the average of the GHG + aerosol simulations. Units °C
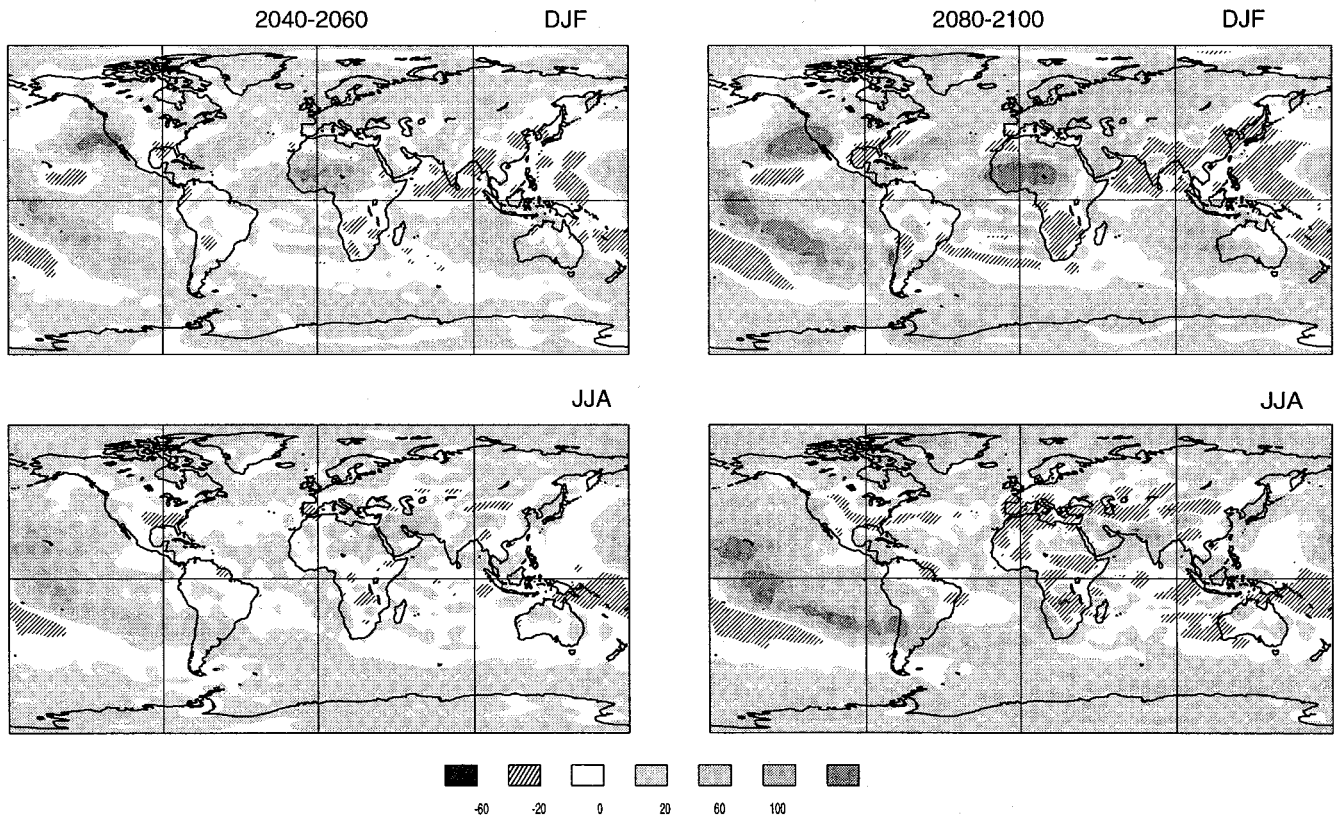
5.6 Mean sea-level pressure

Mean sea-level pressure is an indicator of changes in surface dynamics and to some extent thermodynamics. Figure 19 shows patterns of change which are to some extent characteristic of this model. In particular, the deepening of the Aleutian low in DJF and the general decrease of mean sea-level pressure over much of the Northern Hemisphere and particularly over the continents is generally similar to the $2 \times CO_2$ equilibrium results of Boer et al. (1992) with the AGCM coupled to a mixed layer ocean. While the deepening of the Aleutian low is a feature shared with the $2 \times CO_2$ simulation, in the current simulation the PNA-like pattern across North America is somewhat better developed and there is a shift in mass from east to west in the tropical Pacific connected to the El Nino-like changes in temperature. Despite the strong asymmetry in the simulated surface warming between hemispheres, a similar asymmetry is not reflected in Southern Hemisphere mean sea-level pressure changes which are not dissimilar to the more symmetric mixed layer results and which reflect a modest shift in the Antarctic trough. The general effect of the negative aerosol forcing on mean sea-level pressure (not shown) is, once again, mainly to counteract the broad patterns of GHG forced change. Temperature and moisture changes clearly have the potential of direct social and economic consequences, while changes in

Annual average aerosol effect on temperature

1975-95 to 2040-2060

1975-95 to 2080-2100

■ -6   ■ -4   ▨ -2   ▨ -1   ☐ 0   ☐ 1   ▨

Fig. 16 The effects of aerosol forcing on the annual average temperature for the period from 1975–95 to 2040–2060 and 2080–2100. Units °C

Precipitation change from 1975-95 for GHG+aerosol forcing (%)

Fig. 17 Percentage differences in DJF and JJA precipitation rates from 1975–95 to 2040–2060 and 2080–2100 for the average of the GHG + aerosol simulations

mean sea-level pressure and associated mean winds would seem to have less potential for direct consequences. There may, however, be non-direct implications such as those for ocean productivity (e.g. Hsieh and Boer 1992).
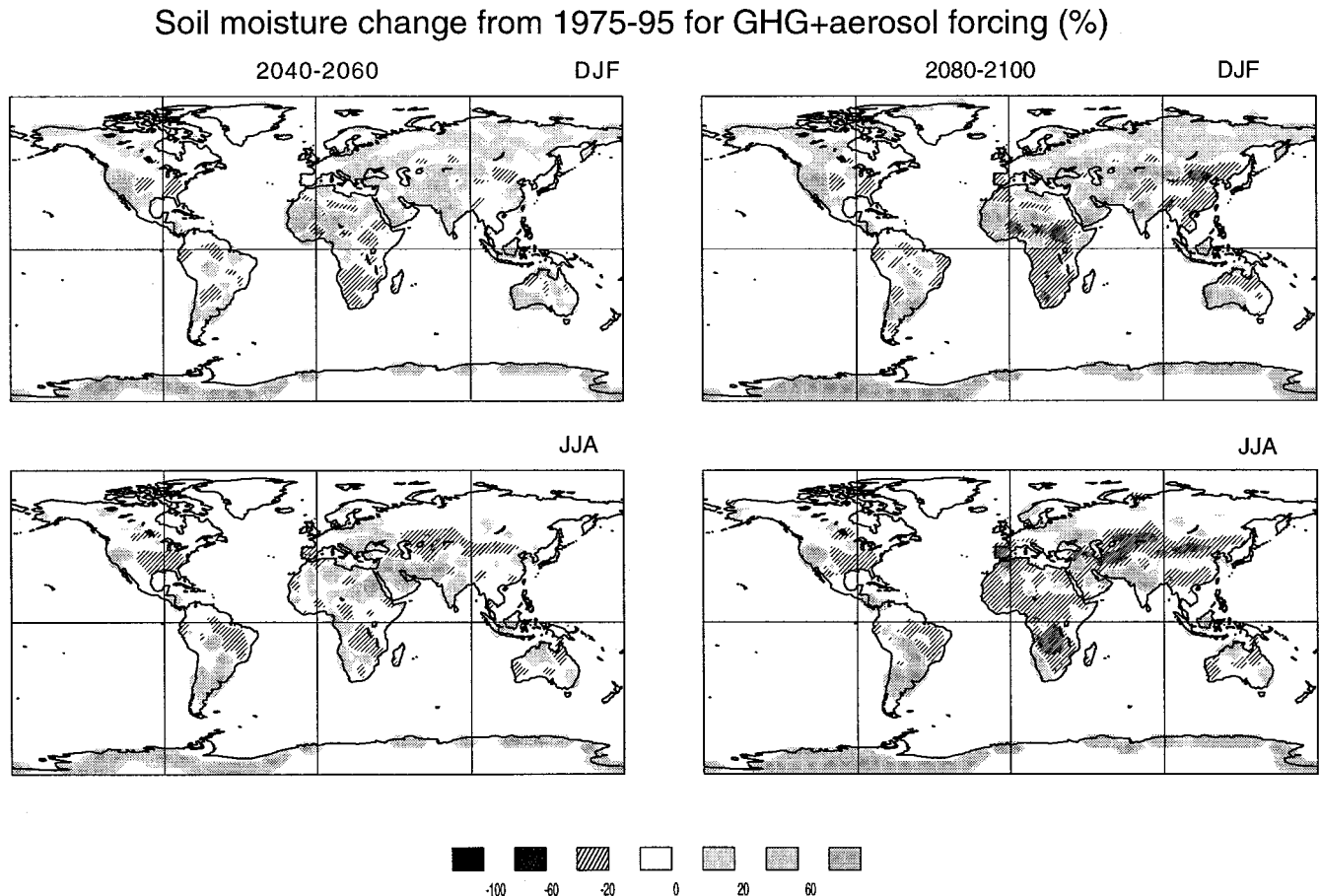
5.7 Thermohaline circulation

The ocean's thermohaline circulation is a major contributor to the oceanic poleward heat transport and a large portion of the Northern Hemisphere transport occurs in the Atlantic. The existence of two or more stable thermohaline circulations for the same climate forcing has been used to explain "rapid non-linear climate change" whereby the current state is replaced by an alternate state with a different and colder northern Atlantic climate. The thermohaline circulation also displays interesting long-time scale variability which may have repercussions for long term climate variability and predictability.

Figure 20 shows the evolution of the maximum value of the annual mean Atlantic overturning stream function for the 1900–2100 period for the control simulation, the average of the three GHG + aerosol simulations, and

the GHG-only simulation. The control run displays variability on a variety of time scales but no pronounced trend with time. This is in sharp contrast to the behaviour of both the average GHG + aerosol and GHG-only simulations. In these cases, the overturning stream function begins a marked decrease in both strength and variability starting at about the present time (this is seen also in the individual GHG + aerosol curves). As has been noted by Manabe and Stouffer (1994), this weakening of the thermohaline circulation and the corresponding poleward transport of heat in the Atlantic is associated with freshening of the north Atlantic by increased precipitation (Fig. 17). It is associated also with a retarded warming/slight cooling in the region seen in the surface temperature (Fig. 15). The implication of this behaviour in the long term is not clear. The behaviour of the overturning stream function differs between models (Rahmstorf 1999) with some showing modest change while others show the kind of changes displayed in Fig. 20.

The decrease in the Atlantic overturning stream function is a change in a dynamical aspect of the ocean climate that affects heat transport and the interaction with the atmosphere. The time scale of recovery of the thermohaline circulation under stabilized conditions is a measure of the "commitment" to oceanic climate change implied by Fig. 20. Manabe and Stouffer (1994) find that the thermohaline circulation recovery depends on the nature and level of GHG forcing at which the system is

Soil moisture change from 1975-95 for GHG+aerosol forcing (%)

2040-2060   DJF   2080-2100   DJF

JJA   JJA

Fig. 18 Percentage differences in DJF and JJA soil moisture availability from 1975–95 to 2040–2060 and 2080–2100 for the average of the GHG + aerosol simulations. Results under the permanent ice caps of Greenland and Antarctica are considered unphysical

stabilized. The behaviour and time scale of recovery of the thermohaline circulation in the current model is under investigation for two "stabilization" scenario simulations with forcing stabilized at years 2050 and 2100.

The Atlantic overturning stream function pattern is displayed in Fig. 18 of Flato et al. (2000) for the control simulation. The "spin-down" of the overturning stream function for the GHG + aerosol simulations is shown in Fig. 21 which indicates: (1) a general slowing which affects the entire Atlantic overturning; (2) a decrease approaching one half of the control value; (3) comparatively little effect due to the negative aerosol forcing. For most climate quantities, the first order effect of the aerosol forcing is to counteract the GHG changes and, if this were the case also for stream function, the bottom panel of Fig. 21 would have the appearance of the upper panels, although with smaller magnitude and opposite sign. This is not the case here, and the aerosol signature, although small, does not have this appearance and is disproportionately confined to high latitudes. Individual GHG + aerosol simulations do not differ from one

another by this magnitude of difference especially for the high latitude maximum.

This illustrates that the north Atlantic meridional overturning stream function, although a major player in the global climate through its role in transporting heat poleward in the Northern Hemisphere, is a comparatively locally forced feature of the oceanic climate. Its response to aerosol forcing is presumably through the local increase in precipitation over the north Atlantic (Fig. 18), which is a localized amplification of the GHG effect, rather than to the more general tendency for the aerosol forcing to counteract GHG changes. The local nature of the forcing of the globally important meridional overturning reiterates the potential sensitivity of this mechanism to future climate change.

5.8 Barotropic stream function

The barotropic stream function is a scaled representation of the depth averaged motions in the ocean. Although not defined locally in the same way as temperature or velocity, changes in barotropic stream function serve to indicate changes to the large-scale oceanic flow. Figure 22 gives an indication of the "signal" in the barotropic stream function in the same way as for the other variables discussed in Fig. 5.1. There is a clear climate change signal in the barotropic stream

Mean sea-level pressure change from 1975-95 for GHG+aerosol forcing (hPa)

2040-2060   DJF   2080-2100   DJF

JJA   JJA
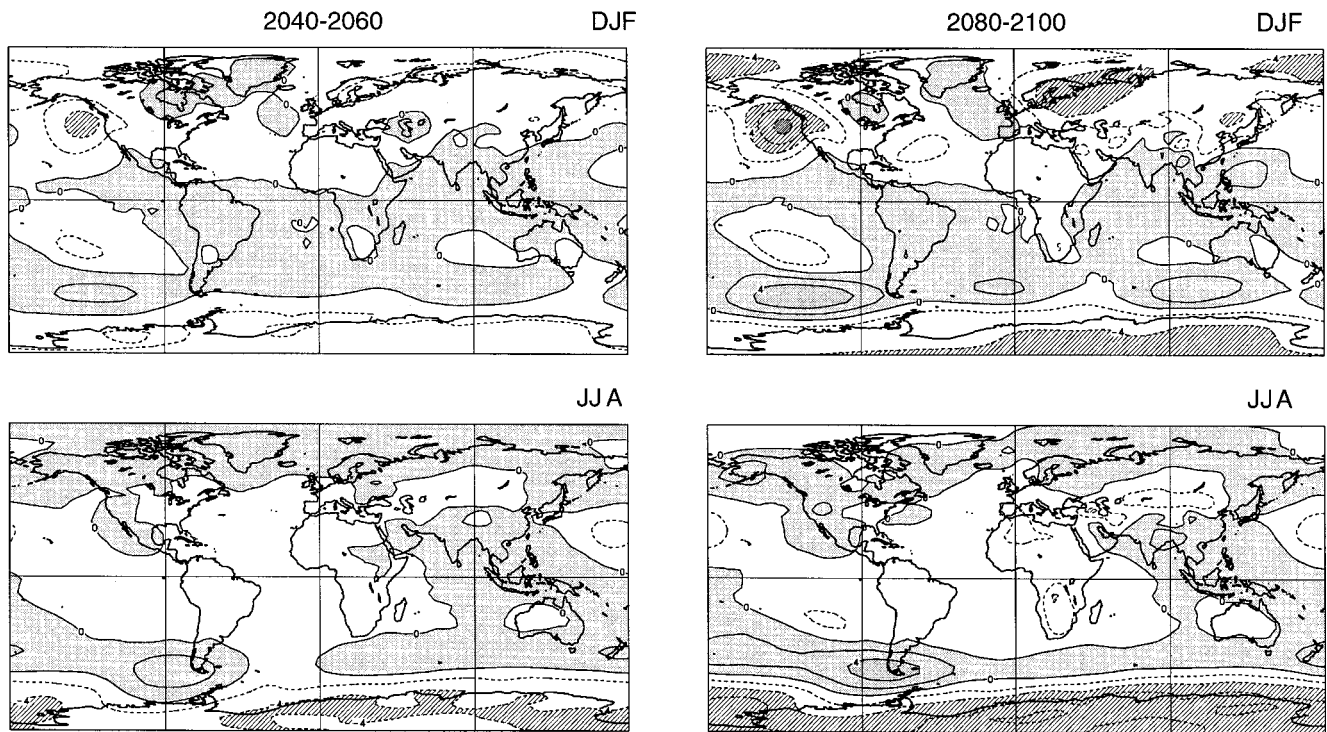
Fig. 19 Differences in DJF and JJA mean sea-level pressure from 1975–95 to 2040–2060 and 2080–2100 for the average of the GHG + aerosol simulations. Units hPa

function although the effect of the aerosols is comparatively modest.

Figure 17 of Flato et al. (2000) gives the barotropic stream function for the control simulation. There is some drift in this quantity which is, however, confined to the margins of Antarctica and does not resemble the kinds of large scale changes seen in Fig. 23 in extent,
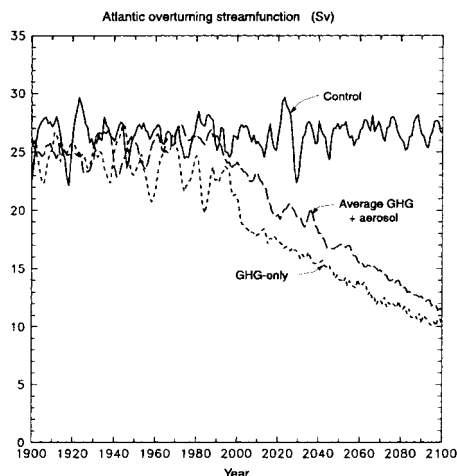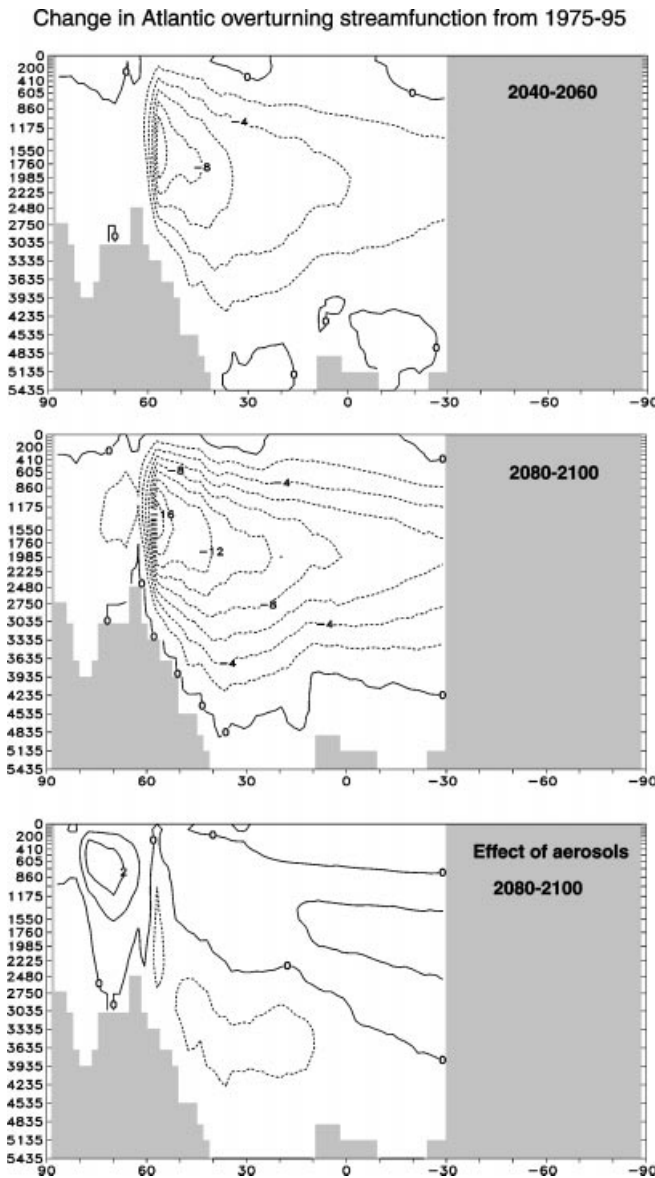
Fig. 20 Maximum of the Atlantic overturning stream function for the control, the average of the three GHG + aerosol, and the GHG-only simulations. Units Sv

pattern or magnitude. The oceanic response to GHG + aerosol forcing is widespread in the Atlantic and in the southern ocean. In the diagrams, the positive (shaded) stream function changes indicate a clockwise circulation change and the reverse for the negative (dotted) regions. The oceanic changes increase as the global warming progresses. In the north Atlantic, the gyre weakens in conjunction with a spin-down of the thermohaline circulation and a reduction in wind stress curl as implied by Fig. 19. Much of the southern oceans undergo changes. The flow changes associated with the El Nino-like behaviour in the Pacific are also apparent. Only the north Pacific is relatively unaffected, at least as far as the barotropic stream function is concerned.

The effect of the negative aerosol forcing is, once again, to counteract the effect of the warming in a broad sense. Since the thermodynamic aerosol forcing is largely localized over land, the dynamic ocean response is clearly indirect. Both the north Atlantic and the southern oceans are regions of small surface temperature change but of comparatively large flow changes. Since the GHG forcing is largely uniform over the globe, these regions must offset the direct forcing by changes in transport and vertical heat exchange to maintain small surface temperature changes.
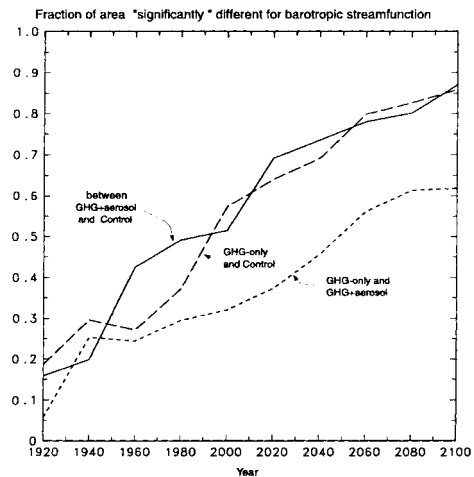
6 Interannual variability

A complete characterization of climate change would include the three-dimensional structure of changes in all statistical moments. In practice, changes in climate

Change in Atlantic overturning streamfunction from 1975-95

Fig. 21 Structure of the changes in the Atlantic overturning stream function from 1975–95 to 2040–2060 and 2080–2100 for the average of the three GHG + aerosol simulations. The *bottom panel* shows the aerosol forcing for the 2080–2100 period. Units Sv

Fig. 22 Fraction of the area of the ocean for which the 20-year means of barotropic stream function are judged to be "significantly different" as measured by the local *t*-test at a nominal 5% significance level. The values are labelled by the final year in the 20-year period

evolution of longer time scale variability and its predictability, all lend impetus to the analysis of changes in variability in simulated climate change.

Various aspects of the change in variability in the simulations described here are investigated elsewhere and include changes in extremes (Kaharin and Zwiers 1999), changes in the AO/AAO (Fyfe et al. 1999) and other modes of variability, and changes in other aspects of variability such as potential predictably. Flato et al. (2000) discuss the interannual variability of the control simulation compared to observations. Changes in interannual variability are discussed here. In particular, for the control simulation the variables are decomposed as $X = X_0 + X^+(t) + X''(t)$ where X^+ is the interannual variation of the monthly or seasonal mean about the climatological value X_0, and X'' is the short time scale variability within the month or season. In order to diminish the effect of the (small) climate drift in temperature in the control simulation, X_0 for that variable includes linear trend. The associated variance is $\sigma_X^2 = \overline{(X - X_0)^2} = \overline{X^{+2}} + \overline{X''^2} = \sigma_m^2 + \sigma_d^2$ where the overbar is the average over the month or season as well as an average over a number of years and/or ensemble members. The first term measures the interannual variability of the means while the second term measures the daily variability about the mean within the month or season.

Attention is concentrated here on σ_m, and in particular on the interannual variability of seasonal means for basic climatological variables. In practice, the DJF and JJA seasonal means are calculated for each year for the period 1900 to 2100 for each of the control, the three independent GHG + aerosol simulations, and the GHG-only simulation. In the case of the forced simulations $X = X_0 + X_f + X^+ + X''$, and the forced component X_f of the climate change at each point is estimated by fitting orthonormal polynomials to third order in

means are given most attention as being both robust and of direct interest. However, changes in variability on various time scales are being given increasing attention despite the associated difficulties which include: (1) the difficulty that models may have in reproducing observed variability on various time scales; (2) the need for longer simulations to investigate variability and its changes; (3) the lack of suitable observational estimates of variability for much of the globe and; (4) the associated difficulty whereby observational error becomes enhanced variability. Nevertheless, the interest in: (1) changes in short time scale variability and especially changes in extremes and extreme events; (2) estimates of variability for climate change detection purposes and; (3) the potential
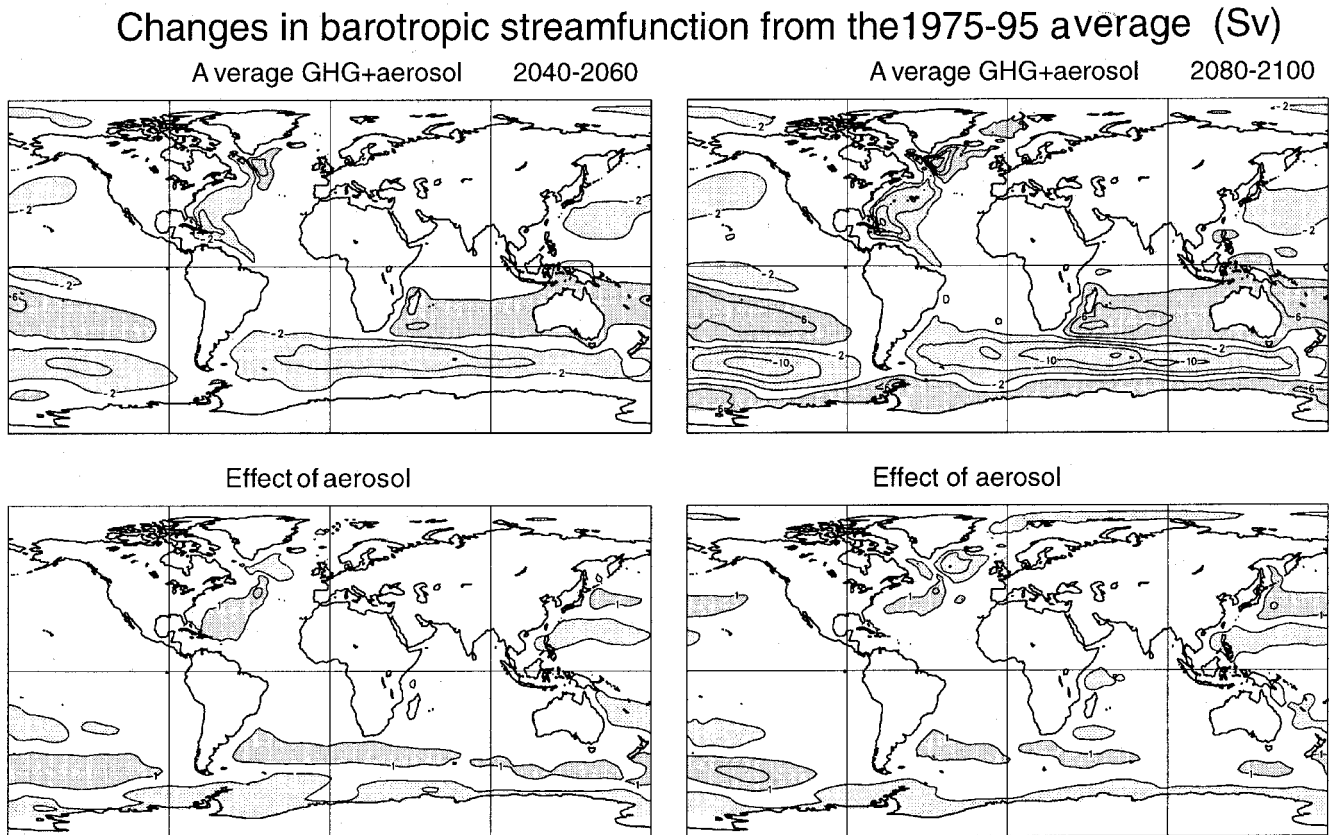
Changes in barotropic streamfunction from the 1975-95 average (Sv)

Average GHG+aerosol 2040-2060 | Average GHG+aerosol 2080-2100

Effect of aerosol | Effect of aerosol

Fig. 23 Changes in the barotropic stream function from 1975–95 to 2040–2060 and 2080–2100 for the average of the three GHG + aerosol simulations. The *bottom panel* shows the effect of the aerosol forcing for the periods. Stream function changes are cyclonic (*dotted negative changes*) or anti-cyclonic (*shaded positive changes*) in the two hemispheres. Units Sv

time. The result is a smooth low order curve at each grid point which fits the long-time scale evolution of the seasonal and annual means. The variation of the individual seasonal means about this curve provides the estimate of σ_m. In the case of the three GHG + aerosol simulations, the estimate of X_f is obtained from the average of the three simulations and the variability about this curve is obtained by pooling all values for the three simulations. The values of σ_m are obtained in this way for four 50-year periods within the 200 year simulations. The F-ratio $F = \sigma^2_{ghg+asol}/\sigma^2_{ctl}$ gives both a visual and statistical indication of where and if the interannual variability of some quantity has changed with respect to the control simulation.

Figures 24 and 25 give the F-ratios for the DJF and JJA interannual variability of surface air temperature, mean sea-level pressure, precipitation, and soil moisture for the last 50-year period of the simulations, namely the period 2050–2100, since these changes are most pronounced compared to the control simulation. The F-ratio gives some measure of the change of interannual variability between the GHG + aerosol simulations and that of the control. Regions of reduced variability are hatched while regions of increased variability are

shaded. Hatched and shaded regions indicate statistically significant changes in variability at the nominal 10% level. The fraction of the globe (or of the land for soil moisture) for which this is the case is given in Table 2. Serial correlation has little effect on variance estimates as discussed in the Appendix of BFRR and is neglected in the calculation.

Temperature and mean sea-level pressure are fields with comparatively large-scale structures and the F-ratios of Fig. 24 are indicative of surface thermodynamic and dynamic variability changes. The diagrams and associated calculations show regions of both increased and decreased variability for temperature and a clear seasonal difference between DJF and JJA changes in the Northern Hemisphere, where temperature variability tends to decrease in DJF and increase in JJA according to this measure. This is understandable for the northern polar ocean and to some extent the adjacent regions where decreasing ice and snow cover damps winter variability but allows summer variability to increase. Areas of (nominally significant) interannual temperature variability increases are matched by areas of decrease in DJF while for JJA areas of increase outweigh areas of decrease. These results agree only partially with the results of mixed layer models summarized in IPCC1995 as indicating an increase of interannual variability in the tropics and subtropics and a decrease at higher latitudes.

Tropical Pacific variability changes in temperature and precipitation imply changes in the nature and variability of the (model's representation of) ENSO. A de-

F-ratios for interannual variability ($\sigma^2_{GHG+asol}/\sigma^2_{Control}$)
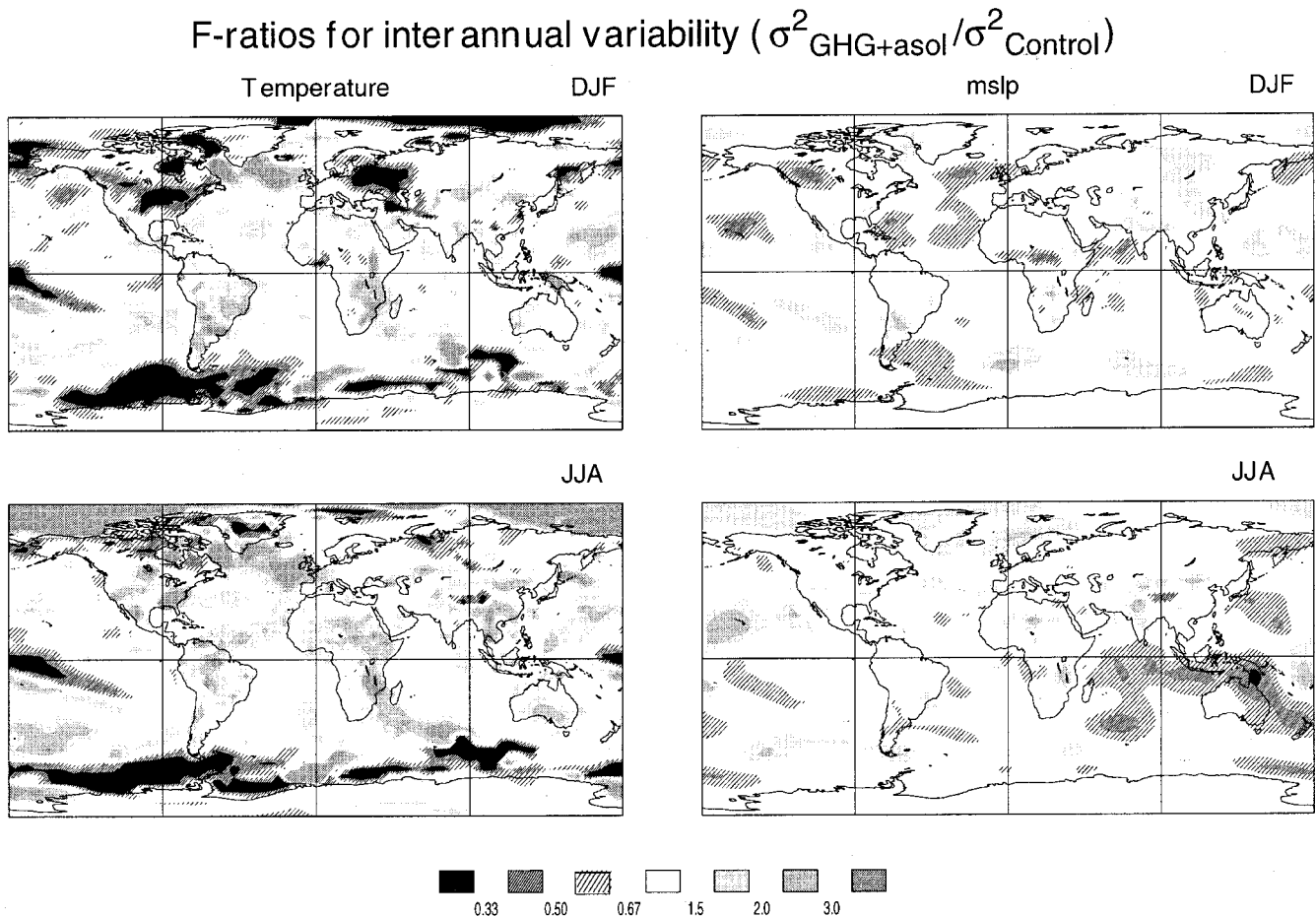
Fig. 24 Ratios of the interannual variance of the DJF and JJA seasonal means for the period 2050–2100 compared to the control simulation for temperature and mean sea-level pressure. Areas significant at the nominal 10% level are *shaded* or *hatched*
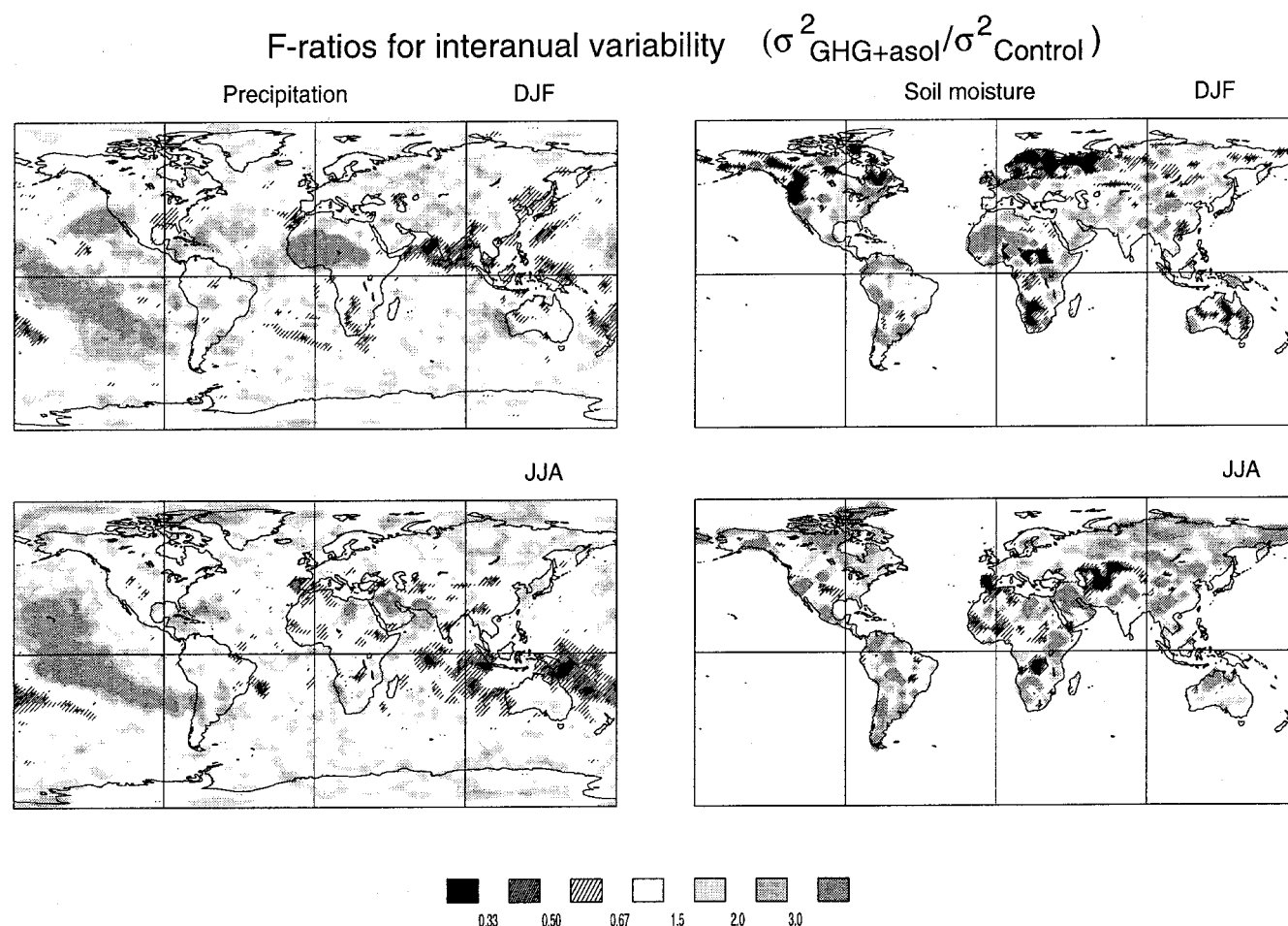
crease in eastern equatorial Pacific temperature variability is associated with an increase in precipitation variability in the warmer climate. These results agree with a subset of results in the IPCC1995 discussion of ENSO variability and change, including the opposing nature of the changes for temperature and precipitation variability, although results are not uniform. It is plausible that the increases in mean temperature in the region (Fig. 15) results in reduced temperature variability due to non-linear increases in processes like evaporation and longwave radiation that act to damp temperature but, if anything, enhance precipitation processes. There is some indication of associated PNA-like changes in variability of temperature, mean sea-level pressure and precipitation values.

Soil moisture in Fig. 25 shows comparatively small-scale patterns of both increase and decrease in soil moisture variability covering a comparatively large fraction of the land area. There is an indication of opposite changes for the two seasons such as the middle latitude decrease in DJF and increase in JJA variability. There is some perceptible connection to the

changes in precipitation variability in certain areas but, of course, the connection is not direct in practice. In particular a decrease in variability may be associated either with an increase in precipitation so that soil moisture levels are always high or alternatively, with a decrease in precipitation so that soil moisture levels are always low. A more detailed investigation of the surface moisture budget is needed to unravel the various possibilities.

The overall picture for changes in interannual variability shows some organized patterns of changes in temperature and precipitation particularly in certain regions of the globe. As expected for a warmer world in which the hydrological cycle is more vigorous, the overall precipitation variability increases. Temperature variability increases and decreases have a seasonal aspect and both temperature and precipitation have variability changes associated with changes in tropical Pacific variability. There are modest change in mean sea-level pressure variability while change in soil moisture variability is widespread.

The same approach is used to test for changes in variability associated with aerosol forcing but there is little evidence of such an effect. More, and more sophisticated, investigations of both interannual and shorter time scale variability are planned using these results as well as those of an extended control run.

F-ratios for interanual variability $(\sigma^2_{GHG+asol}/\sigma^2_{Control})$

Precipitation   DJF   Soil moisture   DJF

JJA   JJA

Legend: 0.33 0.50 0.67 1.5 2.0 3.0

Fig. 25 Ratios of the interannual variance of the DJF and JJA seasonal means for the period 2050–2100 compared to the control simulation for precipitation and soil moisture availability. Results for soil moisture under the permanent ice caps of Greenland and Antarctica are considered unphysical and are not shown. Areas significant at the nominal 10% level are *shaded* or *hatched*

Table 2 Percentage of the area of the globe (or land for soil moisture) exhibiting significant change in interannual variability at the nominal 10% level for the F-test

Variable	DJF	JJA
Temperature	40	44
Mslp	20	28
Precipitation	44	43
Soil moisture	62	68

7 Summary

The CCCma coupled general circulation model is used to investigate the climate effects of increasing greenhouse gas concentrations together with the direct effect of scattering by sulfate aerosols. The experimental design, the control climate, and the simulated and observed aspects of climate change for the twentieth century are considered in two companion papers. Results from five simulations for the years 1900–2100 are available; a control experiment without change in forcing, three independent simulations with increasing GHG plus aerosol forcing, and a simulation with increasing GHG forcing only. The projected climate change to the end of the twenty-first century is discussed.

The rate of climate change accelerates from the present as a consequence of the forcing scenario adopted and the positive feedbacks in the system. Global mean simulated temperatures increase by 1.7 °C from the present to the year 2050 and by a further 2.7 °C degrees by the year 2100. The warming is not uniform and is larger in the Northern Hemisphere compared to the Southern Hemisphere, over land compared to ocean, and in winter compared to summer. The warming is accompanied by a retreat in both snow cover and ice extent, most especially in the Northern Hemisphere. Simulated changes in temperature are statistically robust at least as judged from the *t*-test applied locally at gridpoints. The effect of the comparatively localized aerosol forcing is primarily to counteract the GHG warming signal both as to magnitude and pattern and only secondly to affect temperatures locally thus indicating that the transient climate response is determined to first order by feedback processes in the system and only secondarily by the local pattern of radiative forcing. Finally, a comparison of available simulation results suggests that while it is

possible to distinguish between GHG-only and GHG + aerosol forcing it is difficult to distinguish between results from models with different climate sensitivities until the accelerated warming is well underway.

A general increase in the overall rate of working of the hydrological cycle accompanies the increase in temperature although the acceleration of mean precipitation rate is delayed compared to that for temperature. The effect of the aerosol forcing on temperature also acts to considerably retard the acceleration of the hydrological cycle. Notable changes to the moisture budget include an "El NINO-like" shift in precipitation in the central and western tropical Pacific, a decrease in soil moisture availability especially in Northern Hemisphere summer, and an overall increase in interannual variability of precipitation.

Mean sea-level pressure changes indicate a spin-up of the Aleutian low in northern winter, together with a PNA-like structure apparently associated with the tropical shift in precipitation regime and a slight weakening and shift of the Antarctic trough especially in JJA.

The asymmetry in the warming between the Northern and Southern Hemispheres is a consequence both of the behaviour of the respective oceans in sequestering heat and of the differing distribution of land masses. Oceanic temperature changes show the warming confined largely to the surface especially in the tropics but penetrating to greater depths at high latitudes. The north Atlantic shows little surface warming in conjunction with the spin-down of the thermohaline circulation to nearly half its initial value and a marked decrease in variability. Aerosol effects on the evolution of the north Atlantic thermohaline circulation are comparatively small and differ in that they do not counteract the GHG change but rather have a signature at high northern latitudes in the ocean. This behaviour is associated with aerosol related changes in precipitation in the north Atlantic and reiterates the local sensitivity of this ocean circulation component and, therefore, its potential to play a disproportionate role in future climate change.

The barotropic stream function in the ocean exhibits modest change in the north Pacific but accelerating changes in much of the Southern Ocean and the north Atlantic where the gyre spins down in association with changes in the surface pressure distribution and the associated curl of the wind stress and the decrease in the thermohaline circulation. These changes in flow are those associated with the small, or even negative, surface temperature change found in these regions despite the positive radiative forcing changes that cause warming elsewhere.

Changes in interannual variability show seasonal dependence with Northern Hemisphere temperature variability generally decreasing in DJF and increasing in JJA. There is a shift in tropical eastern Pacific variability apparently associated with changes in modelled ENSO behaviour and a shift also of the variability associated with the Antarctic trough. Mean sea-level pressure variability generally decreases with largest decreases in

the tropical Indian ocean region and both increases and decreases of variability are associated with the ENSO-like change in the Pacific. The interannual variability of precipitation generally increases especially in the central tropical Pacific although there are decreases in the eastern Pacific and Indian regions. Soil moisture variability show widespread and seasonally dependent patterns of variability change.

Climate simulations involving both historical and projected forcing, simulations of increasing length, multiple realizations of climate evolution, and simulations with a range of forcing scenarios are all ingredients of current investigations of past and potential future climate change. The considerable effort of undertaking these integrations and the daunting amount of information produced demands an equal effort in intercomparison and analysis. The results presented here are an attempt to describe, in a more or less hierarchical way, the changes to simulated climate under projected GHG + aerosol forcing changes. These results differ in non-trivial ways from earlier equilibrium $2 \times CO_2$ results with the CCCma model as a consequence of the coupling to a fully three-dimensional ocean model and, of course, to the evolving nature of the forcing.

References

Boer GJ (1993) Climate change and the regulation of the surface moisture and energy budgets. Clim Dyn 8: 225–239

Boer GJ (1995) Some dynamical consequences of greenhouse gas warming. Atmos-Ocean 33: 731–751

Boer GJ, McFarlane NA, Lazare M (1992) Greenhouse gas-induced climate change simulated with the CCC second-generation general circulation model. J Clim 5: 1045–1077

Boer GJ, Flato G, Reader MC, Ramsden D (2000) A transient climate change simulation with greenhouse gas and aerosol forcing: experimental design and comparison with the instrumental record for the 20th century. Clim Dyn 16: 405–425

Cai W, Gordon HB (1998) Transient responses of the CSIRO climate model to two different rates of CO_2 increase. Clim Dyn 14: 503–516

Crow EL, Davis FA, Maxfield MW (1960) Statistics manual. Dover Publications, New York, 288 pp

Cubash U (ed), Caneill J-Y, Filiberti MA, Hegerl G, Johns TC, Keen A, Parey S, Thual O, Ulbrich U, Voss R, Waszkewitz J, Wild M, van Ypersele JP (1997) Anthropogenic climate change. European Commission Rep EUR 17466 EN, 73 pp

Flato GM, Boer GJ, Lee W, McFarlane N, Ramsden D, Reader M, Weaver A (2000) The Canadian Centre for Climate Modelling and Analysis global coupled model and its climate. Clim Dyn 16: 451–467

Fyfe JC, Boer GJ, Flato GM (1999) The Arctic and Antarctic Oscillations and their projected changes under global warming. Geophys Res Lett 26: 1601–1604

Haywood JM, Stouffer RJ, Wetherald RT, Manabe S, Ramaswamy V (1997) Transient response of a coupled model to estimated changes in greenhouse gas and sulfate concentrations. Geophys Res Lett 24: 1335–1338

Hsieh WW, Boer GJ (1992) Global climate change and ocean upwelling. Fish Oceanogr 1: 333–338

Johns TC, Carnell RE, Crossley JG, Gregory JM, Mitchell JFB, Senior CA, Tett SFB, Woods RA (1997) The second Hadley Centre coupled ocean-atmosphere GCM: model description, spinup and validation. Clim Dyn 13: 103–134

Manabe S, Stouffer RJ (1994) Multiple-century response of a coupled ocean-atmosphere model to an increase of atmospheric carbon dioxide. J Clim 7: 5–23

Manabe S, Stouffer RJ, Spelman MJ, Bryan K (1991) Transient response of a coupled ocean-atmosphere model to gradual changes of atmospheric CO_2: part I. Annual mean response. J Clim 4: 785–818

McFarlane NA, Boer GJ, Blanchet J-P, Lazare M (1992) The Canadian Climate Centre second generation general circulation model and its equilibrium climate. J Clim 5: 1013–1044

Meehl GA, Washington WM (1996) El Nino-like climate change in a model with increased atmospheric CO_2 concentrations. Nature 382: 56–60

Mitchell JFB, Johns TC (1997) On the modification of global warming by sulphate aerosols. J Clim 10: 245–267

Mitchell JFB, Johns TC, Gregory JM, Tett SFB (1995) Climate response to increasing levels of greenhouse gases and sulphate aerosols. Nature 376: 501–504

Rahmstorf S (1999) Shifting seas in the greenhouse? Nature 399: 523–524

Reader MC, Boer GJ (1998) The modification of greenhouse gas warming by the direct effect of sulphate aerosols. Clim Dyn 14: 593–608

Von Storch H, Zwiers F (1999) Statistical analysis in climate research. Cambridge University Press, Cambridge, UK

Zwiers F, Kahren S (1998) Changes in the extremes of the climate simulated by the CCC GCM2 under CO_2 doubling. J Clim 9: 2200–2222